Title
Novel Zinc Matrix Nanocomposite as Biodegradable Material with Tunable Mechanical Properties

Author
Liu, Jingke

Publication Date
2020

Peer reviewed|Thesis/dissertation

UNIVERSITY OF CALIFORNIA

Los Angeles

Novel Zinc matrix Nanocomposite as Biodegradable Material with Tunable Mechanical Properties

A thesis submitted in partial satisfaction of the

requirements for the degree Master of Science

in Mechanical Engineering

by

Jingke Liu

2020

ABSTRACT OF THE THESIS

Novel Zinc Matrix Nanocomposite as Biodegradable Material

with Tunable Mechanical Properties

by

Jingke Liu

Master of Science in Mechanical Engineering

University of California, Los Angeles, 2020

Professor Xiaochun Li, Chair

In the past decade, zinc-based biodegradable materials have gained tremendous attention from researchers due to their promising biodegradability and biocompatibility [1] [2]. However, there are several limitations to pure Zn and Zn alloys and their use as biodegradable implants. The most critical drawbacks of pure zinc as biodegradable structural support are its poor strength and low stability, making it unsuitable in most biomedical implant use. This work reports the homogeneous incorporation of WC nanoparticles into the Zn and Zn-Fe matrix as an effective method for mechanical strengthening, namely microhardness strengthening and Young's modulus enhancement. This work also demonstrates the tunability of Zn-WC's mechanical properties and discusses how this tunability makes Zn-WC an ideal candidate for the material

selection of bioresorbable implants. Lastly, this study successfully designed and fabricated a novel high-performance implant spring made of Zn-WC biodegradable nanocomposite for the treatment of short bowel syndrome.

The thesis of Jingke Liu is approved.

Yong Chen

Benjamin M Wu

Xiaochun Li, Committee Chair

University of California, Los Angeles

2020

Table of Contents

TABLES AND FIGURES

Acknowledgment

I would like to thank Professor Xiaochun Li for providing me this wonderful research opportunity at the Scifacturing laboratory. Professor Li offered me beyond significant mentorship and taught me valuable lessons from class to research. I greatly appreciate professor Li's patient guidance, and I hope I can keep getting inspired by his wisdom in the future.

I would like to thank Zeyi Guan, who was the leading Ph.D. student of the biomaterial project. Zeyi taught me a great deal on research techniques and shared knowledge with me generously.

I am very thankful for all the students and visitors in the lab for the memorable time spent together.

I would also like to thank Professor Yong Chen and Professor Benjamin Wu for serving on my thesis committee.

1. Introduction

In the past decade, zinc-based biodegradable materials have gained tremendous attention from researchers due to their promising biodegradability and biocompatibility [1] [2]. Zn exhibits active chemical activity with an electrode potential of -0.762V, which indicates a moderate and suitable biological degradation rate. Also, Zn is a critical element in human nutrition and is considered the second most abundant transition metal element in the human body that helps cell proliferation and the immune and nervous systems [3], [4]. Furthermore, Zinc-based bioimplants release Zn ions that can be integrated into the physiological metabolic activity of the host organism without triggering any toxic systemic side effects [5], [6]. However, there are several limitations to pure Zn and Zn alloys and their use as biodegradable implants. The most critical drawbacks of pure zinc as biodegradable structural support are its poor strength and sustainable plasticity, making it unsuitable in most biomedical implant use [5], [7]–[9]. Although some researchers are attempting to reinforce pure zinc through alloying, there are multiple new mechanical complications and uncertainties due to the low melting point of Zn. Zinc alloys are susceptible to natural aging and static recrystallization (SRX) and thus can cause zinc device failure in room temperature storage and in the applications at human body temperature [10]. Furthermore, different alloy systems may compromise Zinc's biocompatibility as well as its suitable corrosion rate [11].

Recently, the incorporation of nanoparticles into metal matrix has been reported as an effective method for mechanical strengthening due to the Hall-Petch effect and Orowan strengthening

[12]. As our previous study shows, a better balance among biodegradability and mechanical strength can be achieved by introducing uniformly self-dispersed thermally and chemically inert ceramic nanoparticles into Zn [11]. This study successfully designed and fabricated a novel high-performance spring made of Zn-WC biodegradable nanocomposite, which offers enhanced mechanical properties and satisfactory expansion performance that meet the requirement of Short Bowl Syndrome treatment. This work also demonstrates the tunability of Zn-WC's mechanical properties and discusses how this tunability makes Zn-WC an ideal candidate for the material selection of bioresorbable spring implants.

2.Literature Review

2.1 The advantages of zinc as biodegradable material

2.1.1 Biodegradability advantages

Zinc exhibits a moderate degradability rate as Zn degrades slower than rapidly degrading biodegradable Mg and its alloys, yet faster than slowly degrading Fe and its alloys, because Zn produces passive moderately stable layers during corrosion process[5], [13]–[15]. In an arterial environment, for instance, high-purity Zn degrades at tens of micrometers per year, while biocorrosion of Mg can reach hundreds of micrometers per year [2], [16]. According to Bowen et al. [17], the slower biocorrosion rate of Zn comparing to Mg is advantageous because it provides greater metallurgical manipulation freedom because thinner designs can be used when using Zinc, and it permits lower profile implants that reduce post-implant complications. Additionally, when comparing to Mg, Zn does not produce hydrogen by-product in its biocorrosion process [5], [18]. Recently, researchers raised concerns that hydrogen by-product

of in vivo Mg biocorrosion will form gas bubbles around the implant and jeopardize the health of local tissues[19], [20]. When comparing to degradation behavior of ferrous biometals, the degradation of Zn once again appears superior in terms of biocorrosion rate because ferrous biometals degrade at a much slower rate and remain longer than necessary in the body[16]. In addition, ferrous biometals could generate insoluble corrosion products during in vivo degradation, and such insoluble products could be encapsulated by neointima to an enlarged phase to inhibit arterial functions[21]–[24], while Zn does not produce harmful products during degradation. Thus, the suitable biodegradation rate and harmless degradation process of Zn makes Zn an ideal biodegradable metal in biomedical applications.

2.1.2 Biocompatibility advantages

Zn is one of the most abundant and nutritionally essential elements in the human body and is present in most body sections such as skeletal bones, muscles, tissues, organs, and fluids[5], [8], [25], [26]. Zn also plays a crucial role in several physiological aspects including neurosensory development, cell growth, and immune system [4], [13], [27]. The human body has the advanced ability to absorb, consume and excrete zinc, and the requirement for daily intake of Zn is around 15mg[4], [21], [25]. Therefore, Zn becomes a suitable candidate for biometal due to its non-toxicity. Recently, researchers have performed numerous of both in vitro and in vivo tests to determine the actual biocompatibility of Zn in different human body systems. For bones, Zhu et al. [28] suggest that human bone marrow mesenchymal stem cells (hMSC) proliferation and adhesion can be endorsed by Zn biomaterial, and Qiao et al. [29] suggests ionic Zn can stimulate osteogenesis. For vascular cells, Ma et al. [30] suggests low concentration Zn^{2+}, which is a major byproduct release of biodegradable zinc implants, has no adverse effect on vascular cells

(endothelial cells and SMCs) but rather inhibits and promotes cell viability, cell proliferation, cell spreading, and cell adhesion, while high concentration Zn^{2+} has the opposite effect. In vivo studies were also performed to investigate the degradation and intake of Zn ions. Bowen et al.[2], [31] has discovered that the immigration of Zn corroding into the body system was 0.4mg/day to 0.97 mg/day and is far below the Zn daily intake (15mg/day) allowance, suggesting optimal biocompatibility of Zn. In addition, Yang et al. [32]studied pure zinc stent in the animal model and concluded superb biocompatibility without platelet aggregation, thrombosis generation, and severe inflammation after one year. Thus, zinc has advantages in biocompatibility as a biodegradable material and demonstrated significant potential.

2.2 The disadvantages of zinc as biodegradable material

Pure Zn is not exempt from issues and disadvantages. The most major disadvantage of pure Zn is its relatively lower mechanical strength and modulus than both Mg and Fe [16], [33]. Table 1 lists some of the pure zinc's strength and modulus and Table 2 lists some of the mechanical properties of bones and arterial tissues.

Material	**Microhardness [HV]**	**Yield Strength [Mpa]**	**Young's Modulus [Gpa]**	**Reference**
Zn as casted	38	18	64.4	[8], [34]
Zn hot extruded	38	60	-	[8]
Zn-hot rolled	39	50-140		[8], [35]

Table 1. Mechanical properties of pure Zn

Material	Microhardness [HV]	Yield Strength [Mpa]	Young's Modulus [Gpa]	Reference
Cortical bone	-	104.9	5-23	[36]
Cancellous bone	-	-	10-1570(MPA)	[36]
Arterial wall	-	-	1(MPA)	[36]

Table 2 Mechanical properties of surrounding tissues

Since the implantation of biomaterial is employed to substitute and compensate targeted and surrounding human tissues, the mechanical properties of biomaterial should be compatible with the mechanical properties of the tissue accordingly [36]. It is obvious that the inadequate mechanical properties of pure zinc are often considered incompetent for the requirements of most of the bone and arterial medical devices. Therefore, the mechanical properties of Zn, namely the strength and modulus of pure Zn, are fundamentally and urgently needed for the implementation of Zn as a biomaterial.

2.3 Current alloying method for strengthening zinc and its challenges

Due to the low mechanical properties of pure Zn, researchers instinctively turn to an effective way to address the issue by alloying zinc with different elements[37]. The most reasonable approach in selecting alloying elements for biomedical application is to select those that are

known and tested for their biodegradability, biocompatibility, mechanical performances and necessary for human health such as Mg, Ca, Fe, and Cu [16]. Binary alloys were first developed and examined to enhance Zn due to their simplicity. Among all the elements selected for Zn binary alloys, Mg has drawn most of the attention since Mg is the most mature biodegradable metal with some extent of commercial success[38]. Vojitech et al. [7] are the first to discuss Zn-Mg alloy as a potential bone-fixing device, and there has been a significant amount of researches conducted on Zn-Mg system ever since. The typical range of Mg addition varies from 1 to 3%[16]. In addition, researchers have also developed other Zn-based biodegradable alloys system such as Zinc-Iron(Zn-Fe)[37], Zinc-Calcium(Zn-Ca)[8], Zinc-Strontium(Zn-Sr)[8], Zinc-Copper(Zn-Cu)[6], Zinc-Lithium[39], Zinc-Aluminum(Zn-Al)[40], Zn-Manganese(Zn-Mn)[39], and Zinc-Silver(Zn-Ag)[41] Figure 1 illustrates all the binary systems that have been developed since recent years.

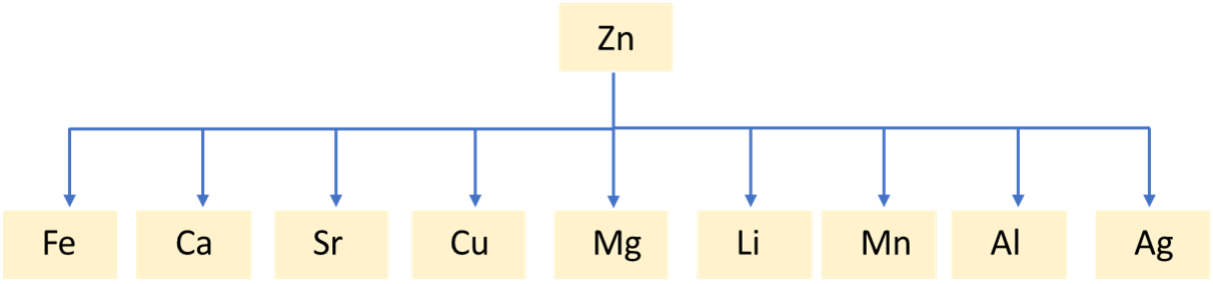

Figure 1 Different Zn binary alloy systems

There are also other ternary alloys systems that use the same selected elements as well, but no new alloying elements were reported so far.

Alloy Composition(wt%)	Microhardness [HV]	Tensile strength [Mpa]	Yield Strength [Mpa]	Reference(from alloy paper)
Zn-1Mg C	70.1±9.6	154.1 ± 15.4	93.4	[7], [42]
Zn-1Mg R	76±3.4	237 ± 20.7	190±11	[43]
Zn-1.5Mg C	95.6±14	149 ± 25.1	112.3±3	[44],[7]
Zn-3Mg C	200±7	84±9	65±9	[45]
Zn-1.3Fe C	56±2	133.6±1.3	80.3±4.6	[33]
Zn-1Ca R	62±2.6	251±9.3	206±9.3	[43]
Zn-1Sr E	73±4.6	223±4.3	134±5.8	[37]
Zn-1Cu E	-	186.3±0.5	147.7±0.5	[46]
Zn-0.1Li R	97±2	274±61	238±60	[47]
Zn-0.2Mn	-	220	132	[48]
Zn-1 Al A&E	73±4.6	223±4.3	134±5.8	[37]
Zn-2.5Ag S	73	261	157	[41]

Table 3 Mechanical properties of different alloy systems

Table 3 shows some of the enhanced properties of Zn based alloy system and it is apparent the strengthening effect of introducing alloying elements was significant. The mechanisms behind strengthening mostly rely on intermetallic phase precipitation strengthening and solid solution strengthening[49].

However, there are several limitations when introducing alloy elements into Zn System. Firstly, the alloying can negatively impact the biodegradability of Zn, as well as the corrosion rate[11]. Secondly, almost all alloying systems with strengthening effects have reported losses of ductility, which can be important for biomedical implant use. Lastly, the biocompatibility of Zinc can be

compromised when less biocompatible elements are introduced into the system and cause more complications[11]. Therefore, a new way to strengthen Zn as a biomaterial is needed.

2.4 Potential Solution to strengthen zinc

2.4.1 Introducing metal matrix nanocomposite (MMNC)

High strength particles reinforced metals received a tremendous amount of attention from researchers to reinforce the mechanical properties of metal matrices[50]. These particle-reinforced metals are recognized as a new class of materials that has "high mechanical strength and other unprecedented properties"[51] and comprehensive researches was conducted in different metal matrices systems. When small-sized particles, namely ceramics microparticles and others, are introduced into relatively soft metal matrices, metal matrix composites (MMCs) were formed, and the properties of metal matrix composites, when comparing to original parent metals, can be enhanced/upgrade significantly[52]. The researches studying on metal matrix composites started gaining momentum since the 1970s when people start to use powder metallurgy and stir casting to incorporate ceramics particles into the pure metal/ alloy systems[53]. Such studies had since reported significant improvement in mechanical properties including Young's modulus, hardness, creep, damping, and wear resistance[54]. These studies had since employed various fabrication and processing techniques to introduce microparticles into the system such as rheocasting[53]. The effort to improve processing of metal matrix composite with microparticles lasted until the new millennium when researchers began to show more interest in nano-sized materials, and they begin to explore the possibilities of using nano-

sized(typically 1-100nm) materials to as strengthening phases in metal matrices, namely targeting Ti, Al, Cu, Mg, and Cu[54], [55]. One of the main reasons why the size of enhancement particles is reduced to nano-scale is that the interaction of fine phases with dislocations is extremely crucial, and the size of nanoparticles plays important role in the effect of reinforcement[56]. In addition, the particle-based damage mechanism of traditional metal matrix composite without nanoparticle reinforcement can cause substandard mechanical properties[53]. The nanoparticles drew the most research interests are predominantly ceramics nanoparticles including oxides, nitrides, carbides, and borides[56]. In addition, other carbon-based nano-sized materials such as carbon nanoplatelets, graphene, and carbon nanotubes have also been used to reinforce not only metal but polymers matrices composites too[53], [57]. When the particles sizes are in the range of nano-size, it is generally believed that the properties of the parent metal could be improved even with a relatively low volume percentage of the incorporated/embedded nanoparticles, and these systems of new materials can be categorized as metal matrix nanocomposite(MMNC)[38]. The following table summarizes all the properties with successful reinforcement that have been reported in various nanocomposite systems.

Enhanced Properties	Reference
Young's Modulus	[50]
Hardness	[11]
Tensile Behavior	[12]
Creep	[58]
Electrical Properties	[50]
Corrosion resistance	[59]
Toughness	[60]

Machining	[61]
Weldability	[62]
Damping	[63]
Wear Resistance	[64]

Table 4 List of enhanced properties reported

Therefore, using nanoparticles to strengthen Zn metal is a feasible way.

2.4.2 Fundamental strengthening mechanism of MMNC

There exist five strengthening effects that contribute to the total yield strength strengthening on metal matrix nanocomposite, and the effects are the Orowan Strengthening effect, CTE mismatch effect, Hall-Patch effect, load-bearing effect, and Young's modulus mismatch effect[53]. Each strengthening effect will be discussed below.

Firstly, the Orowan strengthening contribution is induced by the well-dispersed nanoparticles in the system and can be represented by the following equation[12], [65]:

$$\Delta\sigma_{Orowan} = \frac{\varphi G_m b}{d_p}\left(\frac{6V_p}{\pi}\right)^{1/3} (1)$$

Where G_m is the shear modulus of the matrix, d_p is the size percent of nanoparticles, φ is a constant with a value of 2, V_p is the volume percent of nanoparticles, and b is the Burgers vector. Orowan strengthening is uniquely meaningful in the metal matrix nanocomposite system because this effect can be discarded when the particle diameter exceeds 1 μm[66].

Secondly, the CTE mismatch happens when nanoparticles are stirred into molten metal and the composite is cooled down to room temperature[12]. Typically, the coefficient of thermal expansion(CTE) for nanoparticles are substantially different from the CTE of the metal, and such difference in CTE will cause stress at the particle-metal interface, which will produce

geometrically necessary dislocation(GND)[53]. Then, this GND, like cold working processing, would strengthen the material, and the relationship can be expressed by the following equation[53], [67]:

$$\Delta\sigma_{CTE} = \sqrt{3}\beta G_m b\sqrt{\frac{12V_p\Delta\alpha\Delta T}{bd_P}} \quad (2)$$

Where G_m is the shear modulus of the matrix, V_p is the volume percent of nanoparticles, b is the Burgers vector, ΔT is the absolute temperature difference, $\Delta\alpha$ is the CTE difference between particle and metal, d_p is the size percent of nanoparticles, and β is the dislocation strengthening coefficient. It is worth mentioning that when particles sizes d_p are too small, their contribution to CTE mismatch strengthening can be neglected[68]. In addition, when the cooling rate of molten metal nanocomposite was too slow, the CTE mismatch-induced dislocation GND might get annealed during the cooling, hence eliminating the CTE mismatching strengthening effect[12].

Thirdly, The Hall-Petch strengthening comes mainly from the grain refinement of the metal matrix nanocomposite, which was induced by incorporating nanoparticles into the system[34]. The increase yield strength from grain refinement can be described by the following equation[12]:

$$\Delta\sigma_{H-P} = kd^{-\frac{1}{2}} \quad (3)$$

Where k is a constant and d is the grain size of the nanocomposite. From this equation, we can know that the smaller the grain size is refined by nanoparticles, the stronger the strengthening effect will be. This strengthening effect should be crucial because some studies have reported

significant grain size reductions by nanoparticle incorporation[34], [65]. However, a recent study also suggests that the Hall-Petch effect may lose its function when grain sizes are reduced to around 100nm due to grain-boundary rotation[69].

Fourthly, the load-bearing strengthening effect illustrates the relationship between volume percentage of the nanoparticles and the amount of strengthening, it can be represented in the following equation[12], [53], [70]:

$$\Delta\sigma_{load} = 1.5V_P\sigma_i \quad (4)$$

Where σ_i is the interfacial bonding strength, and V_P is the volume percentage of nanoparticles.

It is noteworthy that most metal matrices contain a low volume percentage of nanoparticles; therefore, this effect is often not a major contributing factor to the whole strengthening effect on the matrix system.

Lastly, the mismatch in Young's modulus between nanoparticles and the metal matrix can also generate strengthening[53]. Nanoparticles used in most metal matrix nanocomposite systems are often ceramics particles, which means these particles often have significantly higher Young's modulus than the base metal. The mismatch in Young's modulus, like the mismatch in CTE, will induce GNDs[67], which will strengthen the nanocomposite. The relationship between modulus mismatch can be expressed in the following equation[67]:

$$\Delta\sigma_E = \sqrt{3}\alpha G_m b\sqrt{\frac{6V_p\varepsilon}{bd_P}} \quad (5)$$

Where ε is the nanocomposite bulk strain and α is the material coefficient. However, for this modulus to match, the nanocomposite must undergo forming (extrusion, rolling, or forging) because the GNDs will only spawn during the forming process of the material.

2.4.3 Hardness strengthening mechanism of MMNC

The hardness strengthening metal matrix nanocomposite can also be explained with the combination of CTE mismatch, Orowan effect, and load-bearing effect and their relationship can be illustrated by the following equation[50]:

$$H = H_0 \cdot (1 + f_{Orowan}) \cdot (1 + f_{load}) \cdot (1 + f_{CTE}) \quad (6)$$

Where H is the composite hardness, H_0 is the metal hardness, f_{Orowan} is the hardness increase factor by Orowan effect, f_{load} is the increase factor due to load-bearing, and f_{CTE} is the increase factor due to the CTE mismatch. Their values can be obtained by the following equations[50], [71]–[73]:

$$f_{load} = \frac{x}{2} \quad (7)$$

$$f_{Orowan} = \frac{0.13Gb}{\lambda \sigma_m} \cdot \ln\left(\frac{r}{b}\right) \text{ with } \lambda = \left(\frac{\pi r^2}{x}\right)^{0.5} \quad (8)$$

$$f_{CTE} = \frac{kGb\sqrt{\rho}}{\sigma_m} \text{ with } \rho = \frac{6\Delta\alpha\Delta T x}{br(1-x)} \quad (9)$$

Where the load-bearing effect factor f_{load} is mainly determined by nanoparticle volume percent x; Orowan effect factor f_{Orowan} depends on Bergers number b, shear modulus G, nanoparticle radius r, the distance between particles λ, and matrix yield strength σ_m; the CTE

mismatch factor depends on the absolute temperature difference ΔT, and the CTE difference between particles and metal $\Delta\alpha$.

2.4.4 Young's modulus strengthening mechanism of MMNC

The Young's modulus can also be enhanced by incorporating nanoparticles into the metal matrix nanocomposite. The enhancement of Young's modulus follows the 'rule of mixture' of composite design, and the modulus enhancement depends on the volume percentage of the nanoparticles into the nanocomposite system. The correlation between Young's modulus and volume percentages can be bound by the following equations[74]:

$$E_{upper} = E_m V_m + E_p V_p \quad (10)$$

$$E_{lower} = \frac{E_m E_p}{E_p V_m + E_m V_p} \quad (11)$$

Where E_{upper} is the upper limit of composite modulus, E_{lower} is the lower limit of composite modulus, E_m is the modulus of the base metal, E_p is the modulus of the nanoparticle, V_p is the volume percent of the nanoparticle, V_m is the volume percent of the base metal.

2.4.5 Nanoparticle dispersion and stabilization in metal matrix nanocomposite (MMNC)

Although metal matrix nanocomposite brings numerous properties improvements and promises unlimited possibilities for future engineering applications, the uniform incorporation of nanoparticles into the metal matrix can be challenging. To achieve desired mechanical properties improvement, reinforcement nanoparticles have to be homogeneously distributed into the system[75]. However, one of the most fundamental issues with metal matrix nanocomposite fabrication is the difficulty to achieve uniform nanoparticle dispersion, because nanoparticles tend to sinter into coarse clusters during liquid metallurgy process due to their non-ideal wettability with molten metal[75].

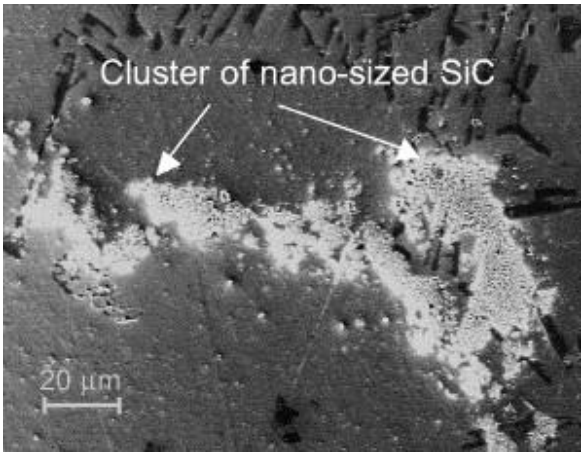

Figure. An example of SiC nanoparticle clusters in aluminum alloy[76]

In addition, researchers found that casting is an attractive way to fabricate metal matrix nanocomposite as a liquid phase process due to its cost-effectiveness, scalability, and ability to process parts with complex geometries[76]. However, the sintering and clustering of nanoparticle clustering is still the main obstacle for liquid metallurgy.

Fortunately, there have been intense researches done on the fabrication techniques in liquid metallurgy and researchers have found different approaches to disperse nanoparticles into molten metal[11], [56], [77]. Here are two popular methods in fabricating the metal matrix nanocomposite.

The first method to incorporate nanophase reinforcements into the metal is through stir-casting. Stir casting is a simpler, faster, and cheaper way to produce metal matrix nanocomposite, and this method is endorsed by many researchers[78], [79]. A typical stir casting has the following set up:

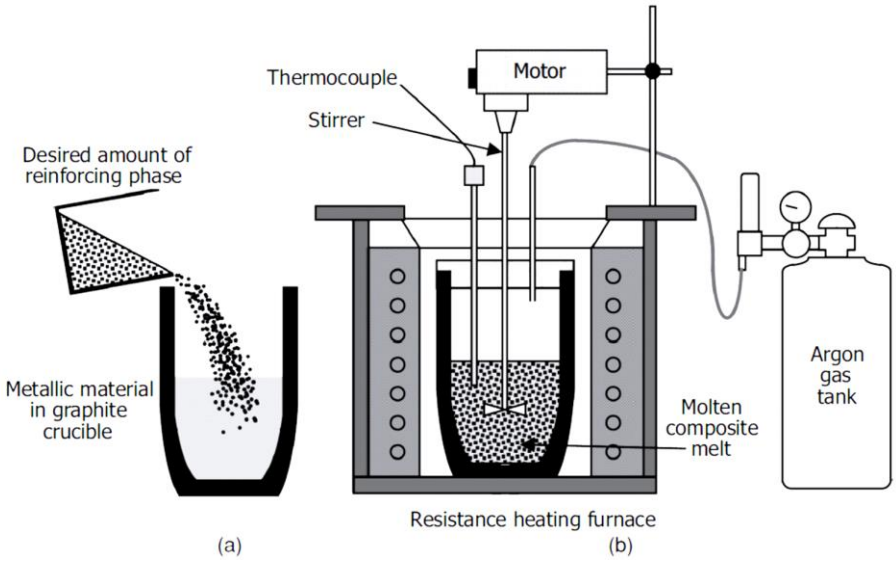

Figure 2 Illustration of a typical stir casting set up[80]

In a typical stir casting set up, a string impeller connected to a motor is inserted into the molten metal melt to create vortex flow of the molten metal, which is designed to help with the dispersion of the nanoparticles. This method is straightforward, and the force created by the impeller, which mainly depends on the string rate and the viscosity of the metal slurry, which depends on the system temperatures and mixture density, are the two main

factors that determine the homogeneity of the nanoparticles dispersion in stir casting[79]. However, this stir casting method has some shortcomings including increase amount of gas porosity from the stir-generated turbulence, and a high chance for nanoparticles to clusters owing to insufficient mixing and high van der Waals force[53].

More recently, researchers have come up with a novel way to help disperse nanoparticles into the matrix more uniformly by using ultrasonic processing to help with incorporation[76]. They have found that by using high-intensity ultrasonic waves, they could generate non-linear effects in molten metal liquid. This use of ultrasonic waves into the liquid can generate acoustic streaming and transient cavitation[81], and such effects can help nanoparticle dispersion in the molten metal.

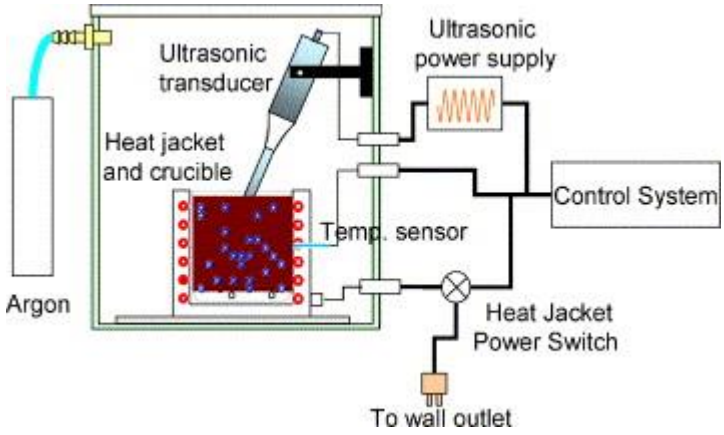

Figure 3 Aluustration of a typical ultrasonic processing setup [76]

This figure shows a typical set up of ultrasonic processing during nanocomposite fabrication. The implementation of the ultrasonic transducer is proved to be a tremendous success in dispersing nanoparticles into different metal matrices including aluminum and magnesium system[12], [52], [81].

In addition, researchers have recently found the self-dispersing and self-stabilizing mechanism of nanoparticles in molten metal[12]. They have found that through a combination of reduced van der Waals forces between ceramic nanoparticles in molten metal, a high energy barrier stopping nanoparticles from sintering due to fair wettability between nanoparticles and molten metal, and a high nanoparticle thermal energy, self-stabilization of homogeneous dispersion could be achieved[12], [50].

There exists a van der Waal attraction between two ceramic nanoparticles in molten metal, and the attraction between two particles can be approximately described by the following equations[82]:

$$W_{vdw}(D) = \frac{\left(\sqrt{A_p}-\sqrt{A_m}\right)^2}{6D}\left(\frac{R_1 R_2}{R_2+R_2}\right) \quad (12)$$

Where A_p are the Hamaker constants of ceramic particles, A_m is the Hamaker constant of the molten metal, D is the distance between two particles, and R_1 and R_2 are the radius of the two nanoparticles. It is worth mentioning that this equation is only meaningful when the distance between the two nanoparticles is closer than two atomic layers[12]. If the distance between the nanoparticles is smaller than two atomic layers of the metal, the interaction between two nanoparticles would be dominated by a much stronger interfacial chemical bond in the interfacial energy composition[82].

The thermal energy of nanoparticles in the metal matrix composite system determines if the nanoparticles can escape from the inherent van der Waals attraction and therefore separate from each other. The thermal energy E_b can be calculated from the following equation:

$$E_b = kT \quad (13)$$

Where T is the temperature and k is the Boltzmann constant. The energy, if larger than van der Waal's attraction, can keep nanoparticles from clustering together.

Another energy that prevents nanoparticles from sintering and clustering is the Energy barrier. When ceramics nanoparticles contact each other in a high-temperature environment such as in molten metal, they tend to sinter together. When two ceramics nanoparticles get close to a distance of 0.2nm, the atomic layer of metal will be squeezed out, and the particle surfaces will replenish the original metal-particle interface, causing an interfacial energy surge[12]. This increase in interfacial energy can be described in the following equation[12]:

$$W_{barrier} = S(\sigma_p - \sigma_{m-p}) = S\sigma_m cos\theta \quad (14)$$

Where σ_p is the nanoparticle surface energy, σ_{m-p} is the interfacial energy between molten metal and nanoparticle, S is the effective area, σ_m is the molten metal surface tension, and θ is the contact angle between the molten metal and nanoparticle. This equation suggests that when the wettability of a nanoparticle in a metal matrix is poor, which means a higher contact angle θ, the lower energy can prevent the nanoparticles from sintering. Therefore, when picking designing a metal matrix nanocomposite system, a better wettability of nanoparticle should be considered with priority, because a smaller contact angle will provide a naturally high energy barrier will ensure more homogeneous dispersion of nanoparticles without clustering and sintering.

3. Material Design

3.1 Nanoparticle selection

From the literature review part, we conclude that the incorporation of nanoparticles into the Zn matrix system serves as an effective way to strengthen metal Zn with great potential. However, selecting the right nanoparticle can be challenging.

There are several criteria that need to be considered when selecting the right nanoparticle for the Zn matrix nanocomposite.

Firstly, the most critical property of nanoparticles in MMNP is the wettability between the ceramics nanoparticles and the molten Zn. Low wettability of ceramics nanoparticles will intuitively prevent the homogeneous dispersion of particles in the matrix, because nanoparticles, often in small powder form, have a tendency to aggregate and form clusters in molten metal[56]. The failure to achieve homogeneity will defeat the very purpose of employing nanoparticles into the system, which is to strengthen the mechanical properties of the base metal. Although some fabrication methods could be used to help with the dispersion of nanoparticles, it is inherently dependant on the wettability between particles and molten metal that determines the feasibility of the match. In other words, advanced fabrication techniques would not matter if the selected nanoparticles are naturally unwettable in certain metal and alloy. The fundamental reason for the generally poor wettability between ceramics nanocomposite and the metal is that ceramics are mostly bonded by the ionic or covalent bond in nature and are not compatible with metallic famalies[83]. The low wettability between

nanoparticles and metal is also due to the high surface tension of the molten metal[34]. In order for the nanoparticle to wet into the metal, the adhesion energy between the metal melt and ceramics should be reasonably larger than the molten metal surface tension[83].

Secondly, the nanoparticles must be inert and stable to be considered as reinforcement agents of metal matrix nanocomposites. The main reason for such requirement is that during the fabrication process, especially during the melting and casting process, the nanoparticle should remain chemically inactive with the system. This particular requirement cast no challenges for most of the ceramics nanoparticles since most of them (carbides, oxides, and borides) are quite inert and stable by nature. Even some particles tend to be more active than others, several prevention methods will often take place to protect the nanoparticles from reacting.

Thirdly, the nanoparticle selected should be thermally stable. Liquid processing of metals such as casting is often in high-temperature environments. Therefore, the nanoparticles should be thermally stable in the system. Some nanoparticles are prone to oxidation when thermally treated and should not be considered in high-temperature processing.

Therefore, a suitable nanoparticle as reinforcement in Zn should have the following qualities: reasonably good wettability in molten Zn, chemical inertness, and thermal stability.

Tungsten Carbide (WC) emerges from the nanoparticles to a suitable candidate for Zn strengthening. Firstly, researchers have found out that WC exhibits good wettability with Cu and its alloy due to the reasonably low surface tension of molten Cu, especially with alloying elements sufficiently altering the surface tention[50]. Liquid Zn, on the other hand, has a

surface tension even lower than the liquid Cu. The table compares some of the properties of liquid Zn and Liquid Cu.

Material	Surface tension	Density	Reference
Liquid Zn	1.339	8.02	[50]
Liquid Cu	0.750	6.57	[84]

Table 5 A comparison between liquid Zn and Liquid Cu

Since the higher the surface tension is the main factor undermining the wettability and countering the adhesion energy between ceramics nanoparticles and molten metal, a low metal surface tension is a good indication of fair wettability. There is a lack of direct fundamental study on WC nanoparticles wetting mechanism in Zn. However, it is proven that WC nanoparticles have fair wettability in Cu, which has substantially higher liquid surface tension than Zn. Therefore, it is logical to assume an inherently fair wettability between WC and Zn.

In addition, the high melting point of WC (3143 K) indicates good thermal stability and excellent resistance to oxidation when placed under a high-temperature environment[85]. Also, WC exhibits excellent chemical inertness, as well as high mechanical properties such as high Young's modulus (530 Gpa)[86] and Vicker hardness(2600 HV)[85]. Therefore, WC nanoparticle is a suitable candidate for strengthening the Zn matrix.

3.2 Base material selection

It is obvious that the main purpose of selecting nanoparticles suitable for the Zn matrix is to strengthen Zn and this work will discuss the strengthening effect of WC nanoparticles on pure Zn matrix.

However, this work also novelly explores the possibilities of strengthening Zn-based alloy by incorporating WC nanoparticles into the alloy system. Specifically, this work studied the strengthening effect of nanoparticle reinforcements on the Zn-Fe alloy system.

As discussed before, alloying has been employed as an alternative method to strengthen the mechanical properties of pure Zn while pure Zn was criticized for its lack of adequate mechanical strengths for load-bearing applications[39]. Magnesium(Mg) and iron(Fe), becomes the immediate choices of alloying elements because Mg and Fe are already adequate candidates for biodegradable metals.

Iron as an element has proven its biocompatibility and has a good reputation for not provoking inflammatory responses from the immune system[87]. Recently, Zn-Fe emerges as a new biocompatible alloying option for Zn-based biomaterial. Researchers have discovered that the use of Fe as an alloying element could tune the corrosion rate of zinc through a micro-galvanic effect while maintaining post-implantation biodegradation integrity and biocompatibility[88]. Therefore, Zn-Fe emerges as a biological feasibly option for an alloy.

More importantly, relatively low content of Fe in the Zn matrix can strengthen the mechanical properties of Zn through the intermetallic precipitate effect. When different Fe element is

added into the Zn system, secondary phases will be formed. Researchers, for instance, have found the $Zn_{11}Fe$ phase when 1.6 wt% of Fe is alloyed into the Zn matrix, and strength and hardness were effectively reinforced[33].

Figure 4 shows the phase diagram of the Zn-Fe alloy system.

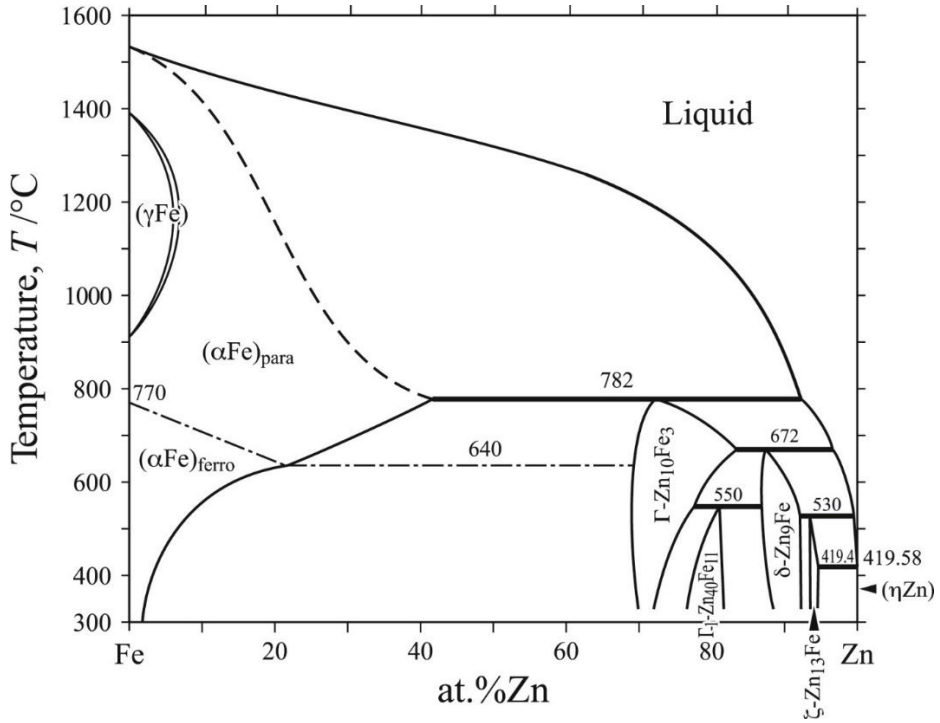

Figure 4 Zn-Fe phase diagram [89]

This work designs for a system with a Zn-Fe alloy system with 2wt.% iron reinforced with WC nanoparticles. The iron content will produce the intermetallic phase participates in the system, which will mechanically enhance the matrix. In addition, the WC nanoparticle will further enhance the microhardness and Young's modulus of the matrix. Thus, a novel Zn-based nanocomposite with tunable mechanical performances will be fabricated, namely the Zn-Fe-WC matrix nanocomposite.

4. Experimental Procedures

4.1 Fabrication of Zn-WC nanocomposite

Salt assisted stir-casting was used to fabricate Zn-WC nanocomposite.

Firstly, WC nanoparticles (50-200nm) was mixed with potassium aluminum fluoride ($KAlF_4$) salt at a 1:10 volume ratio for later use. The purpose of this pre-mixing is to tune the wettability between WC nanoparticles and Molten Zn. Molten potassium aluminum fluoride salt has different interfacial energy between Zn than WC particles. Therefore, by mixing potassium aluminum fluoride salt with WC nanoparticles, we could employ the salt as a delivery agent for WC nanoparticles since molten salt will help with the wettability and therefore achieve a more homogeneous nanoparticle dispersion. Figure 5shows the mixing process of WC nanoparticles with potassium aluminum fluoride salt. The thorough mixing of the two materials is critical for later incorporation because the pre-clustering of WC nanoparticles is undesired. Therefore, a mechanical shaker was used to ensure a total mixture of salt and nanoparticles.

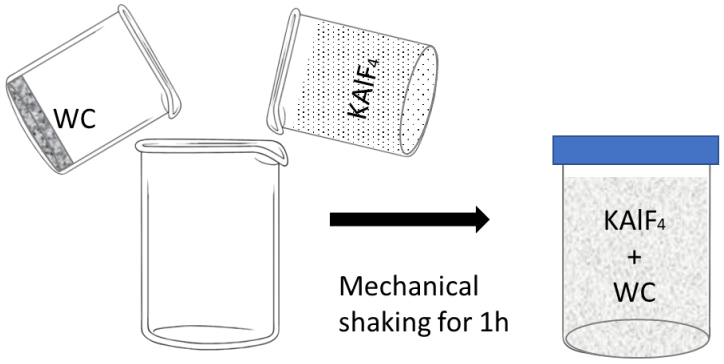

Figure 5 Illustration of salt-nanoparticle mixing

After mixing the WC nanoparticles and potassium aluminum fluoride salt. 30 g of pure potassium aluminum fluoride salt was added to a 3-kg graphite crucible, this salt is melted in an induction furnace at 800 °C. This salt is used as a protection layer for later Zn melting. Zn is easily oxidated during melting and Zn oxides are unwanted in Zn-WC nanocomposite. The density of molten salt is way lower than molten Zn, so the molten liquid salt will float at the surface of molten Zn to completely eliminate oxygen contact. This function of salt was traditionally performed by argon protection, but argon often does not protect Zn well enough and sometimes causes unwanted turbulence at the metal liquid surface. Then, 500 g of pure Zn pellets(99.9%, RotoMetals) were carefully added into the salt melt. The induction furnace was kept at 800 °C for 5 min to ensure complete melt of Zn, which has a melting temperature of 419.53°C[90]. Then, a graphite stirrer connecting to a motor was set up. The impellers were positioned at the interface between salt and metal. The placement of the impeller is critical because if the impeller is placed in metal, the system is going to be severely disturbed and metal and salt will not separate from each other during the casting process. Later results part will discuss the outcome of the wrong placement of impeller. The graphite stirrer was set to have a stirring speed of 400 rpm. Then, the pre-mixed WC-$KAlF_4$ powders are gradually added into the system. Each adding is incremental because the added salt needed to be fully melted before more mixture can be added to ensure the best quality. Figure 6 is an illustration of the process

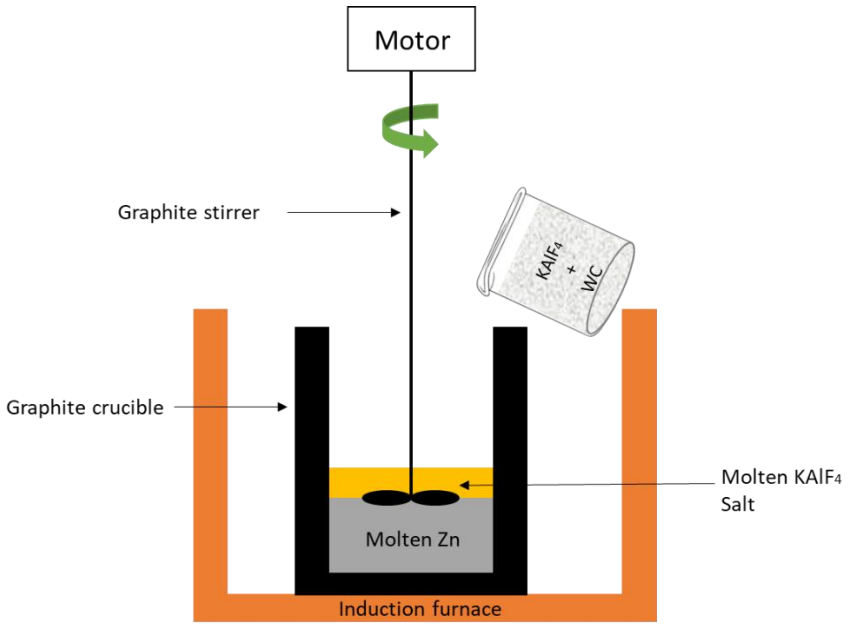

Figure 6 Illustration of experiment setup

After all the WC-salt mixture was added, the system is kept at 800 °C and 400 rpm for 1 h to ensure the dispersion of nanoparticles.

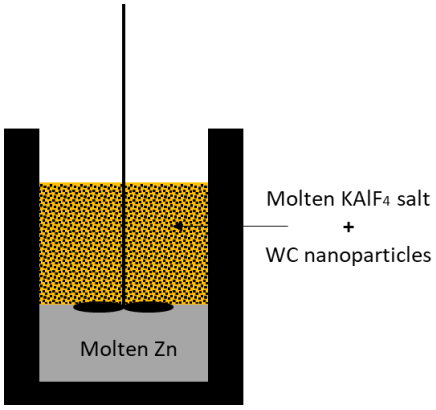

Figure 7 nanoparticle incorporation

Figure 7 illustrates how WC nanoparticles are incorporated into the molten Zn.

Then, ultrasonic processing was performed to help with the nanoparticle dispersion and salt entrapment elimination. The $KAlF_4$ salt was cast out first since the remaining WC nanoparticles

made it too dense. KCl salt was added and melted as an oxygen induction layer during ultrasonic processing.

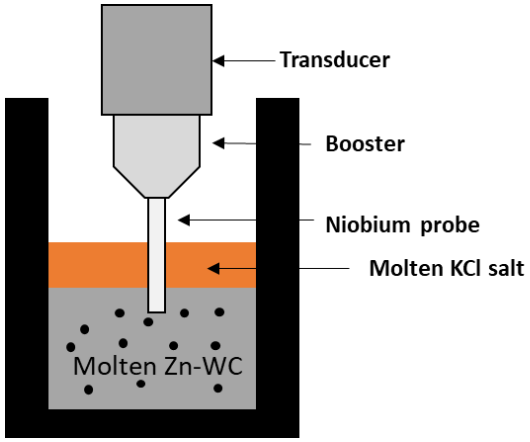

Figure 8 Illustration of ultrasonic processing of Zn-WC

Then, the salt on the surface was cast out and Zn-WC was cast into a preheated (150 °C) steel mold into Zn-WC plates 9mm thickness. The reason for the heated mold is to eliminate cracking from casting.

Salt was selected to help with the incorporation process for three reasons. Firstly, molten salt on top of Zn can protect Zn from severe oxidization. Secondly, molten salt can tune the interfacial energy between particles and metal, therefore increase the wettability. Lastly, the salt and pre-disperse the nanoparticles. The direct adding of nanoparticles into the high-temperature system without salt will cause sintering of nanoparticles immediately, and salt can be a buffer and great intermediate agent during the incorporation process.

4.2 Fabrication of Zn-Fe-WC nanocomposite

The fabrication of the Zn-Fe-WC nanocomposite is similar to the fabrication of Zn-WC. The main difference is that Fe pieces (Alfa Aesar, 99%) were added to the crucible after the incorporation of WC.

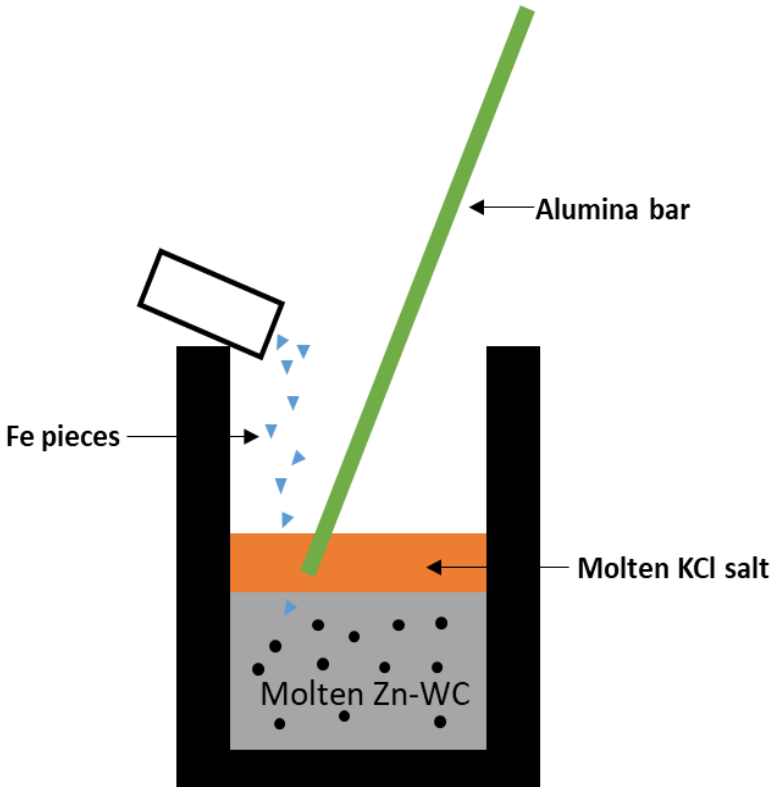

Figure 9 Illustration of Alloying Fe with Zn-WC

Figure 9 illustrates how Fe pieces are alloyed into the Zn-WC system. The pieces are so fine(20µm) that they tend to flow in the salt. An alumina bar was used to manually press the Fe pieces into the Zn melt to make sure Fe stayed there and melt with Zn. Then the crucible is kept at 800 °C for 20 min before salt was removed and samples were cast into plates.

4.3 Sample preparation

All of the casted samples are in shapes of thick plates (10cm *5cm*0.9cm). For later examination and categorizations, these plates, both Zn-WC and Zn-Fe-WC, are hot rolled into thin plates. The hot rolling reduction ratio is 1:2 each run, and each run was performed multiple times to ensure reduction precision. The 0.9 cm plates were hot rolled 4 runs to achieve total reduction ration of 16:1 to 560 μm. Then, these thin sheets were hot rolled into 400 μm thick thin sheets for later categorization.

Wire electrical discharge machining (wire EDM) was employed to cut these thin sheets into small sample sizes(1cm*1cm*400 μm).

These small samples are later mounted onto polishing mounts and polished to 1200 grids on SiC polishing paper. Alumina powder solution was used lastly for final polishing on polishing cloth. These samples were later ion-milled since Zn is inherently soft and WC particles can be ground off from Zn-WC and accumulate on the sample surface. All of these samples were later immersed in acetone and ultrasonic processed for 1 hour to clean the polishing residue off the surface.

4.4 Microstructure characterization

All samples were first observed under an optical microscope first to examine the proficiency of polishing, salt entrapment, porosity, and preliminary nanoparticle dispersion. Then, these samples are mounted on stainless steel mounts with conducting tape. Scanning electron microscopy(ZEISS supra 40VP SEM) will be used to further investigate the dispersion of WC nanoparticles in the system and the surface morphology of the sample. Energy-dispersive X-ray (EDS) was used to confirm the volume composition of the sample, as well as to confirm the dispersion of WC in Zn.

4.5 Microhardness characterization

Microhardness testing was done on different samples with LM 800AT microhardness tester with 200gf load and 10 second dwell time.

4.6 Young's modulus characterization

Young's modulus was tested on an MTS Nanoindenter XP of different samples with different nanoparticle concentrations. The penetration depth was set into the surface 2000 nm at 45 Hz and with a 0.05 s^{-1} strain rate.

5. Results and Discussions

5.1 Microstructures

5.1.1 Microstructures of Zn-WC

As discussed before, when the impellers were placed incorrectly in the crucible, namely too far into the molten metal, the entropy in the molten liquids will be too high. In other words, molten liquid Zn will be scattered as into molten salt as small pieces. The chaotic status of the salt of the metal will lead to a casting catastrophe. The first trials of the incorporation show the failed results. These failed as casted plate are shown in figure 10

Figure 10 Failed cast sample

From figure 10 we can observe that molten metal and salt are intertwined with each other. To avoid such disappointment, the stirring setup is the most crucial parameter to control. After a process of trial and error, the best results are reached when the rpm is set to 400-600 rpm with stirred placed exactly at a metal-salt interface.

The successful casting samples are shown below:

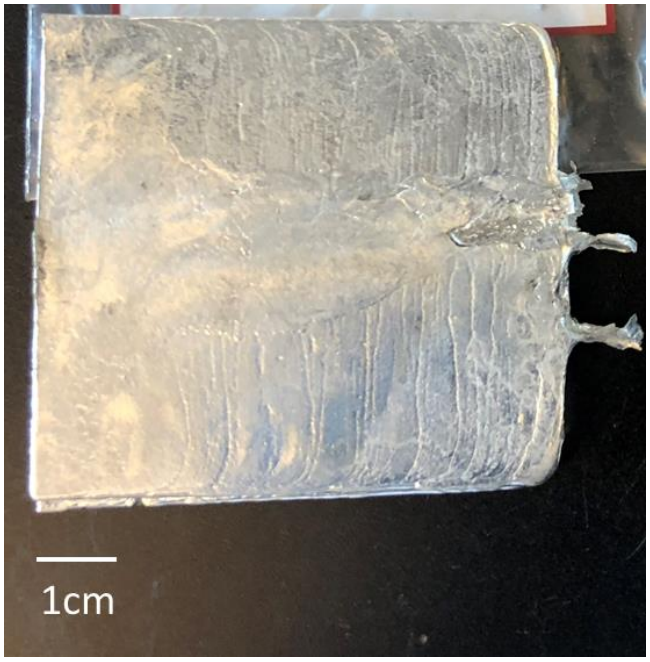

Figure 11 Zn-WC cast sample

Figure 11 shows a result of a successful casting with no visible cracking. These samples were later annealed for 2 hours at 250°C for better hot rolling results; since the thickness reduction ratio was rather high, annealing was needed to increase the ductility to avoid cracking, especially when there are potential salt entrapments in the sample.

Figure 12 shows the hot rolling samples.

Figure 12 Hot-rolled Zn-WC thin sheets

These thin slabs of zinc were later cut and polished to be observed for the microstructures.

Figure 13 shows the microstructure of the Zn-5Vol.% WC sample under different magnifications of an optical microscope.

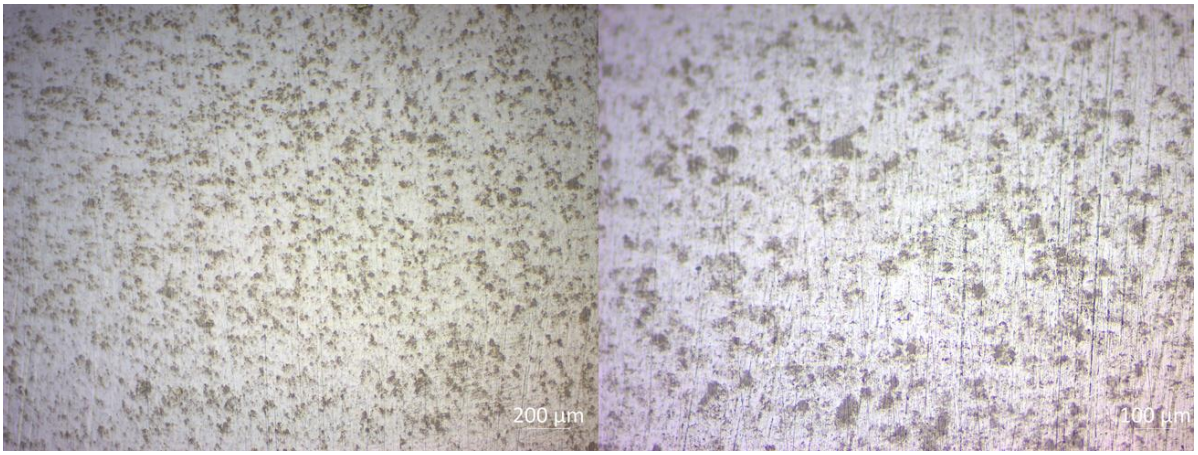

Figure 13 WC nanoparticle dispersion under an optical microscope

In these figures, the white phases are the Zinc base material, and the darker phases are incorporated WC nanoparticles. The distribution of the WC nanoparticles is fair through a preliminary investigation through optical image investigation. Later, these samples are placed under a scanning electron microscope to further confirm the dispersion of WC nanoparticles and the composition of the material.

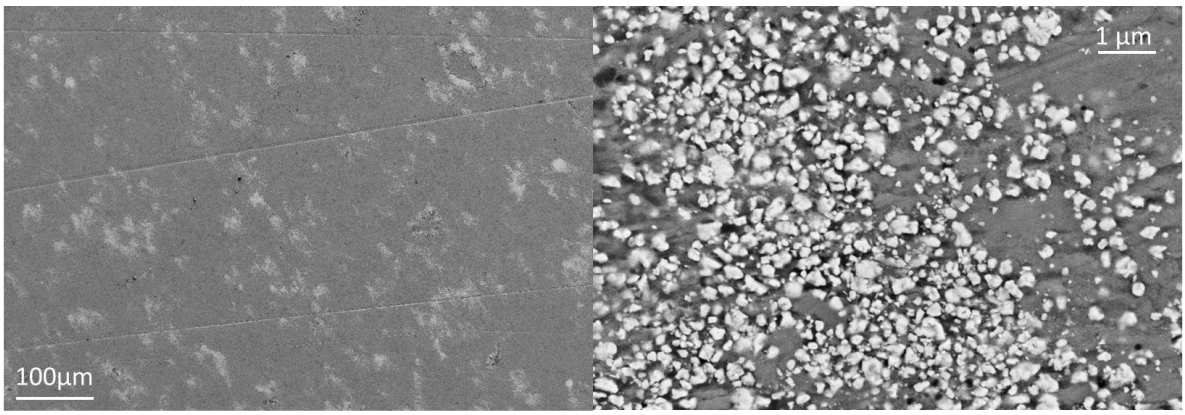

Figure 14 SEM images of WC nanoparticle dispersion

In figure 14, SEM images are shown under different magnifications. The brighter phases are WC nanoparticles, while the darker background is the metal base Zn. The dispersion of nanoparticles are fairly homogeneous throughout the entire sample

Figure 15 confirms the sizes of WC nanoparticles and confirms no sintering effect between individual nanoparticles. The black holes are dents of original nanoparticles that got polished off or brushed off during the ion-milling process

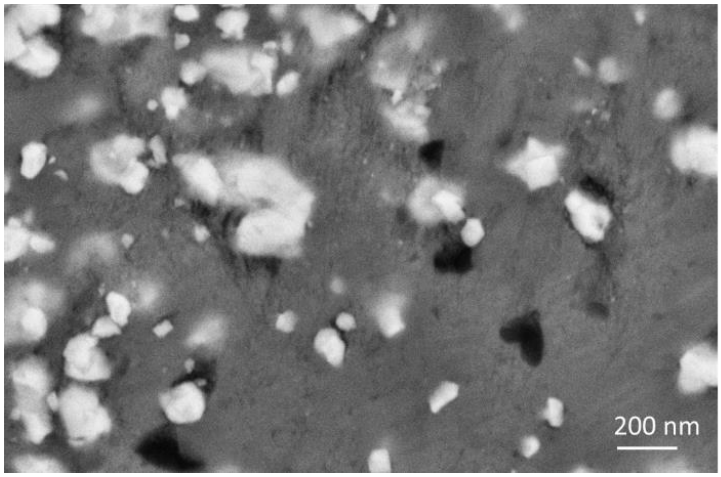

Figure 15 SEM of WC nanoparticles in Zn system

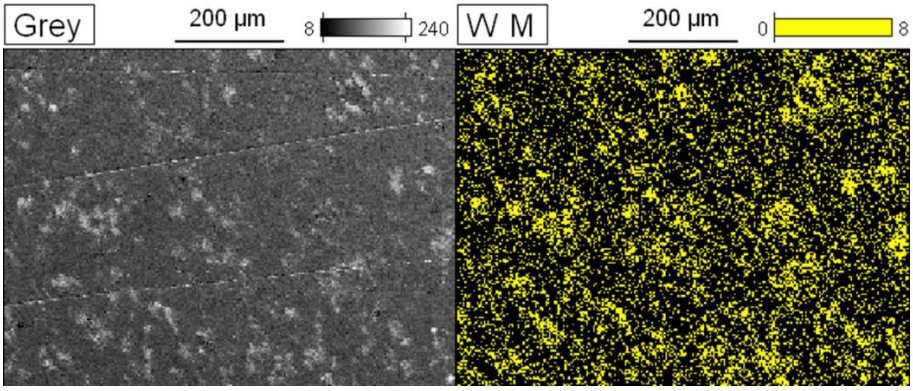

Figure 16 EDS mapping of Zn-WC

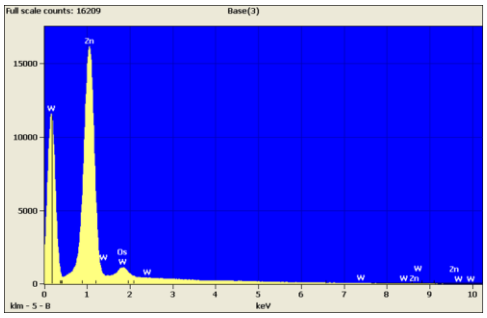

Element Line	Counts	Net Wt.%	Element Error	Wt.%	Atom % Error	Atom %
Zn K	217	---	---	---	---	
Zn L	139759	85.69	+/-0.61	94.46	+/- 0.67	
W L	0	---	---	---	---	
W M	8962	9.23	+/-0.44	3.62	+/- 0.17	
Os L	0	---	---	---	---	
Os M	4791	5.08	+/-0.34	1.93	+/- 0.13	
		---		---		

Figure 17 EDS mapping results

Figure 16 shows the Energy-dispersive X-ray (EDS)of the sample and confirms that the white phases to be WC nanoparticles. In addition, the EDS scan on the sample confirms the weight percentage of W to be 9.23%. Given that the densities of W, WC, and Zn, through calculations, the volume percentage of WC is 4.98 volume percent, which is close to the designed 5 volume percentage of WC nanoparticles.

Therefore, this fabrication of the Zn-WC nanocomposite is successful.

5.1.2 Microstructures of Zn-2Fe-WC 2

The successful cast and rolled samples of Zn-Fe-WC sample are shown in figure 18

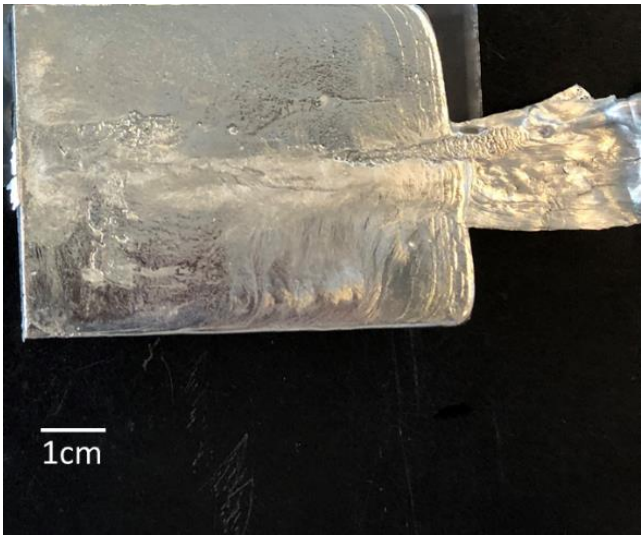

Figure 18 Casting sample of Zn-Fe-WC

The samples were annealed and hot-rolled as well. The surface morphology under the microscope is shown in figure 19.

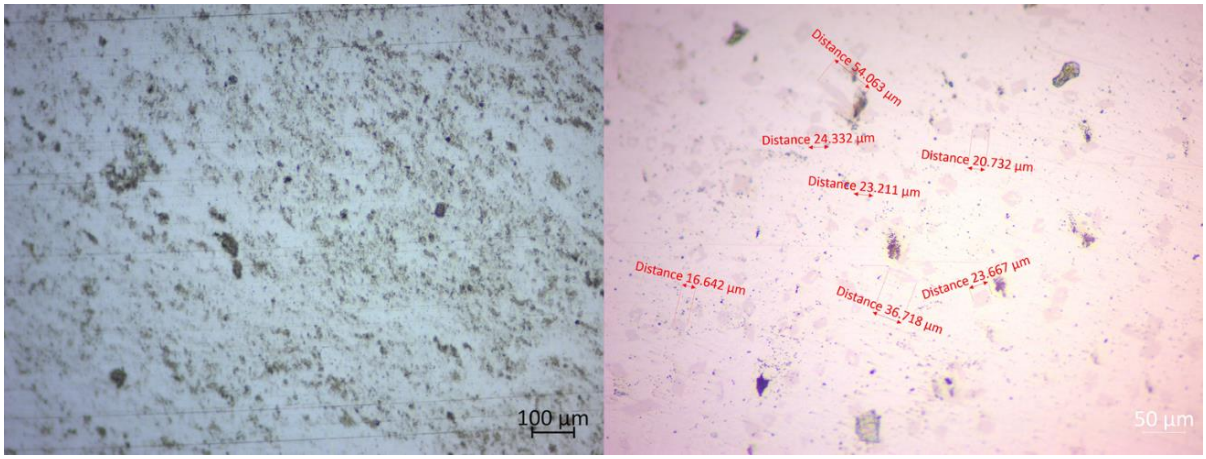

Figure 19 WC nanoparticle dispersion under an optical microscope

The intermetallic phases are found and measured in sizes. The darker phases are WC nanoparticles and the brighter background is Zn. These intermetallic phases are $Zn_{13}Fe$ from the phase diagram.

A scanning electron microscope (SEM) was used to further investigate the distribution of nanoparticles. The brighter phases are WC nanoparticles and the darker background is the Zn-based materials.

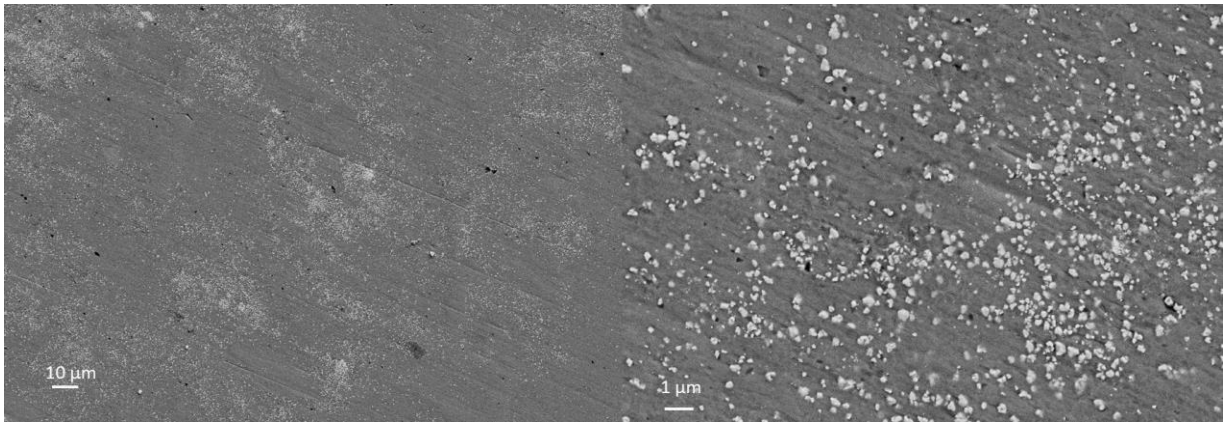

Figure 20 SEM of WC nanoparticles dispersion in Zn system

Figure 20 shows that the distribution of WC nanoparticles is homogeneous in the Zn base metal and there is no sintering effect between individual WC nanoparticles.

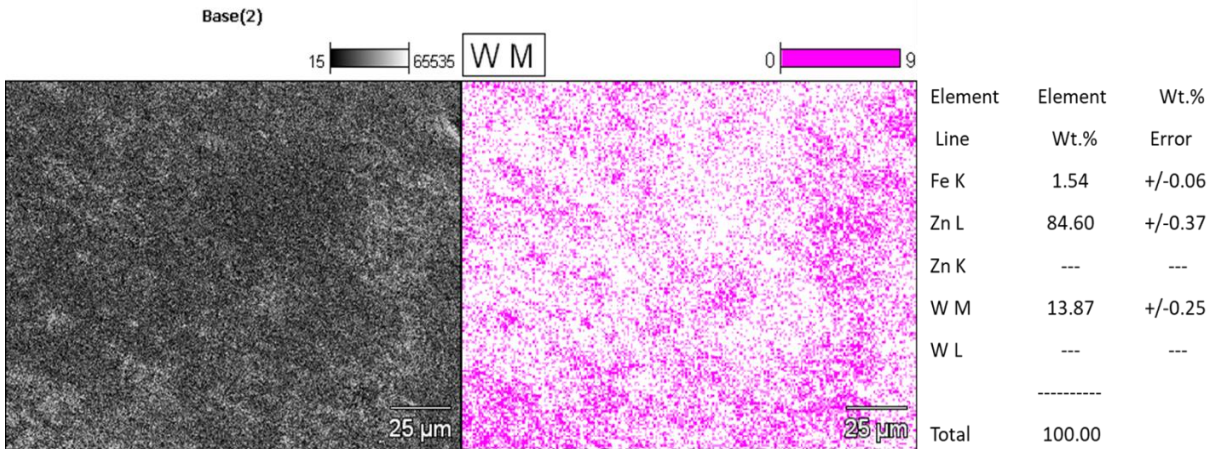

Element Line	Element Wt.%	Wt.% Error
Fe K	1.54	+/-0.06
Zn L	84.60	+/-0.37
Zn K	---	---
W M	13.87	+/-0.25
W L	---	---

Total	100.00	

Figure 21 EDS mapping of Zn-Fe-WC

Figure 21 shows an EDS mapping of the sample and the brighter phases are confirmed to be WC nanoparticles. The weight percent of W is confirmed to be a 13.87%, which is 7.2 volume percent, which is close to designed 5 volume percent considering the selected region is slightly denser. Then weight percent of Fe is confirmed to be 1.54%, which is close to designed 2 weight percent of Fe.

Therefore, the fabrication of Fe-2Fe-5WC is considered successful with homogeneous dispersion of WC nanoparticles.

5.2 Microhardness Enhancement

The microhardness of each Zn-WC sample was measured and compared with Pure Zn samples fabricated under the same circumstances (Cast and hot-rolled)

Each material has 3 samples and each sample was tested at 5 different points to get the average representative values.

Material	Microhardness[HV]	Standard Deviation
Pur Zn	38.025	1.35
Zn-5WC	52.275	2.51

Table 6 Microhardness results

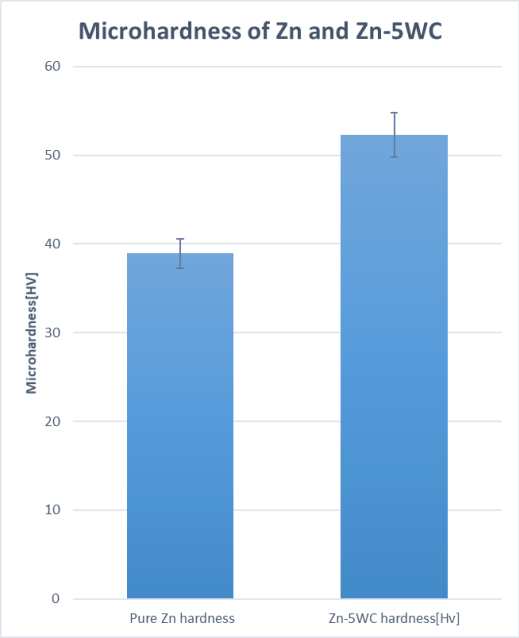

Figure 22 Microhardness comparison between Zn and Zn-WC

Table 6 and figure 22 shows the results of microhardness testing on different materials. From the experiment results, we get that with homogeneous incorporation of 5 volume percent of WC nanoparticles, the microhardness of Zn has increased 37.48%, from 38.025 HV to 52.275

HV. Such an increase in hardness is significant considering Zn was traditionally regarded as a soft metal with relatively low hardness.

The reason for the enhancement in microhardness is due to the combination of Orowan effect and load-bearing effect. The relationship can be expressed by equation x-y.

The microhardness of each Zn-Fe-WC sample was measured and compared with Pure Zn samples and Zn-Fe alloy samples fabricated under the same circumstances (Cast and hot-rolled)

Material	Microhardness[HV]	Standard Deviation
Pure Zn	38.025	1.35
Zn-2Fe	47.842	1.36
Zn-2Fe-5WC	59.119	2.01

Table 7 Microharness results of different systems

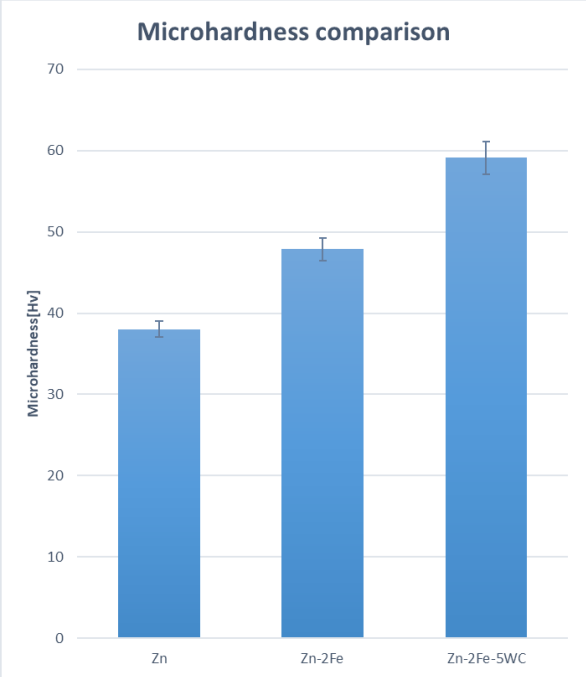

Figure 23 Microhardness comparison between Zn, Zn-WC, and Zn-Fe-WC

Table 7 shows the results of the microhardness testing of the Zn-Fe alloy and Zn-Fe-WC nanocomposite comparing to pure zinc. The alloying of 2 weight percent iron into the system

has strengthened the hardness by 25.82%, from 38.025 HV to 47.842 HV. The additional 5 volume percentage of WC nanoparticles has increased the alloy hardness by 23.58%, from 47.842 HV to 59.119 HV. The microhardness of the Zn-Fe-WC nanocomposite has increased by 55.47%, from 38.025 HV to 59.119 HV. By incorporating merely 2 weight percent of iron and 5 volume percent of WC nanoparticles, the microhardness of the material has been strengthened more than half. The strengthening effect of alloying comes from the intermetallic participate phases $Zn_{13}Fe$, and the strengthening effect of nanoparticles comes from the combined effects mentioned earlier in the chapter. More importantly, the main contributing factor of microhardness is the load-bearing effect[50], which is determined by the volume percentage of the nanoparticles in the system. Therefore, by simply incorporating different volume percentages of WC nanoparticles, the hardness of Zn-based nanocomposite can be tuned to different application needs.

5.3 Young's Modulus enhancement

The Young's modulus of each Zn-WC sample was measured and compared with Pure Zn samples fabricated under the same circumstances (Cast and hot-rolled)

Material	Young's Modulus[Gpa]	Standard Deviation
Pur Zn	71.4	9.8
Zn-5WC	80.9	12.1

Table 8 Young's Modulus measurements

The reason for the strengthening effect is mainly from the rule of mixture; WC nanoparticles, which have extremely high Young's modulus, when thoroughly and homogeneously dispersed in the Zn matrix, will inherently increase the system's modulus. The high standard deviation comes from the measuring method nanoindentation because small disturbance of the measuring environment can cause this particularly delegate measuring method to have a large deviation. To ensure the accuracy of measuring, 9 points of measurement is done on each sample.

To further prove the enhancement effect of WC nanoparticles on Zn despite rather large data deviations, different samples with different WC volume percent were produced and examined to prove a positive correlation between WC nanoparticle content and Young's modulus.

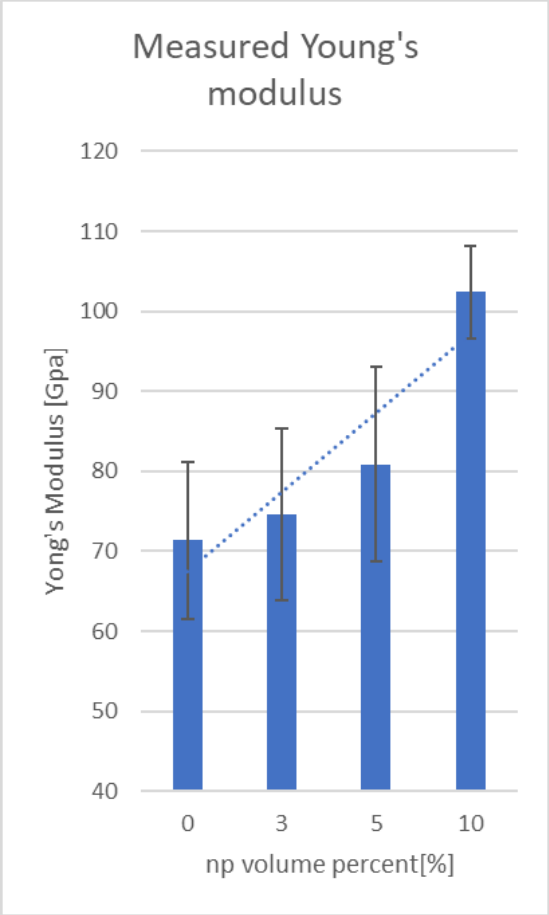

Figure 24 Zn-WC Young's modulus with different WC volume percent

Figure 24 clearly shows a positive trendline relationship between nanoparticle content and Young's modulus. In other words, more WC nanoparticles will enhance Young's modulus of Zn-based nanocomposite.

The Young's modulus of the nanocomposite can be predicted to fall in the bounds proposed by equation (10) and (11) .

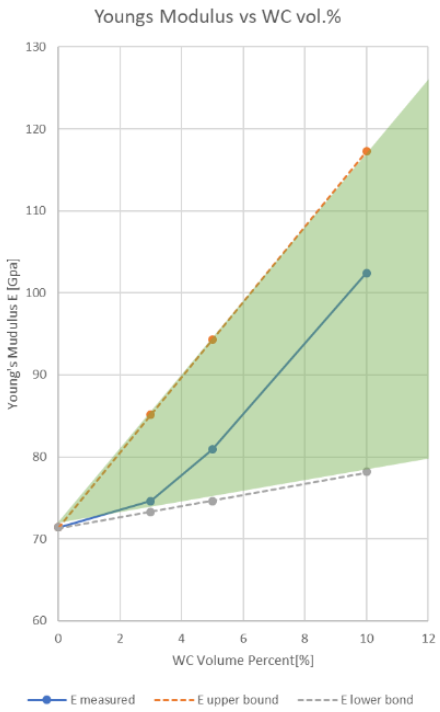

Figure 25 Zn-WC Young's modulus with different WC volume percent vs prediction values

Figure 25 shows that the measured Young's modulus is reasonable and falls into the prediction bounds of the rule of mixture.

Therefore, by incorporating different volume content of nanoparticles into the metal Zn, one can enhance and tune Young's modulus of the material. This tunability opens a gate for vast possibilities of biodegradable implants with different mechanical demands.

6. Potential Applications

Short Bowel Syndrome (SBS) is an enervating condition where the small intestine is too short and thus unable to absorb an adequate amount of nutrients because of the decreased absorptive area [91]. Current treatments for SBS include total parenteral nutrition, small bowel transplantation, and recombinant growth hormone. However, these treatments are not always effective and transplantation availability is limited [92]. Recently, there has been promising research and testing conducted regarding the utilization of endoscopically inserted polymer and nitinol springs to elongate the small intestine [93] [4] [5]. However, these polymer and nitinol based springs are permanent and must be surgically removed from the body after they have successfully elongated the bowel. Thus, there is a great need to find a new material that can not only satisfy the mechanical requirements of spring implant but can also degrade inside the body without harmful effects.

As our previous study shows, a better balance among biodegradability and mechanical strength can be achieved by introducing uniformly self-dispersed thermally and chemically inert ceramic nanoparticles into Zn [11]. This study successfully designed and fabricated a novel high-performance spring made of Zn-WC biodegradable nanocomposite, which offers enhanced mechanical properties and satisfactory expansion performance that meet the requirement of Short Bowl Syndrome treatment. This work also demonstrates the tunability of Zn-WC's mechanical properties and discusses how this tunability makes Zn-WC an ideal candidate for the material selection of bioresorbable spring implants.

To fabricate spring wires, hot rolling of the Zn-WC disk was performed at 200°C with a thickness reduction ratio of 20:1 from 9mm plate to obtain 450µm thin plates. Wire-electrical discharge machining (wire-EDM) was used to cut thin plates into rectangular-cross-section (450µm x 500µm) wires with suitable length. All wires were grounded to 600-grit grinding paper, followed by ultrasonic cleaning in acetone. These wires were later coiled onto a mandrel with a 15mm diameter mounted on a lathe to make suitable spring samples for spring constant measurements and future in vivo testing of porcine subjects. Some wire segments were prepared by 1200-grit grounding paper and then alumina nanoparticle polishing for later microstructure characterization, microhardness tests, and nanoindentation tests.

Microstructure characterization was carried out by optical microscopy, scanning electron microscopy (SEM) (a ZEISS Supra 40VP SEM), and energy-dispersive X-ray spectroscopy (EDS). An LM 800AT microhardness tester was used to test wire microhardness with a 200gf load and a 10 second dwell time. For Young's modulus measurements, an MTS Nanoindenter XP was employed to test samples with different nanoparticle concentrations (penetration depth into surface set to 2000 nm at 45 Hz and 0.05 s^{-1} strain rate).

The typical microstructure of the Zn-WC wires used to fabricate biodegradable spring is shown with different magnifications in Figure 1. The darker particle phases are single crystalline WC particles and the brighter phases are Zn. A wire sample was observed from the optical microscope after polishing to show a homogeneous dispersion of WC nanoparticles in wires with no serious sintering. When zoomed 100 times under a microscope, nanoparticles can be seen clearly apart from each other with individual shapes' outlines matching the sizes of the

original nanoparticles (~200nm). This distribution is achieved by mechanical stirring, as well as the good wettability between molten Zn and WC enabled nanoparticle self-dispersion [11], [96]. Figure 1d gives an overlook of WC nanoparticle distribution along the wire in a 5.5mm polished segment which confirms the incorporation of dispersed nanoparticles throughout the entire wire.

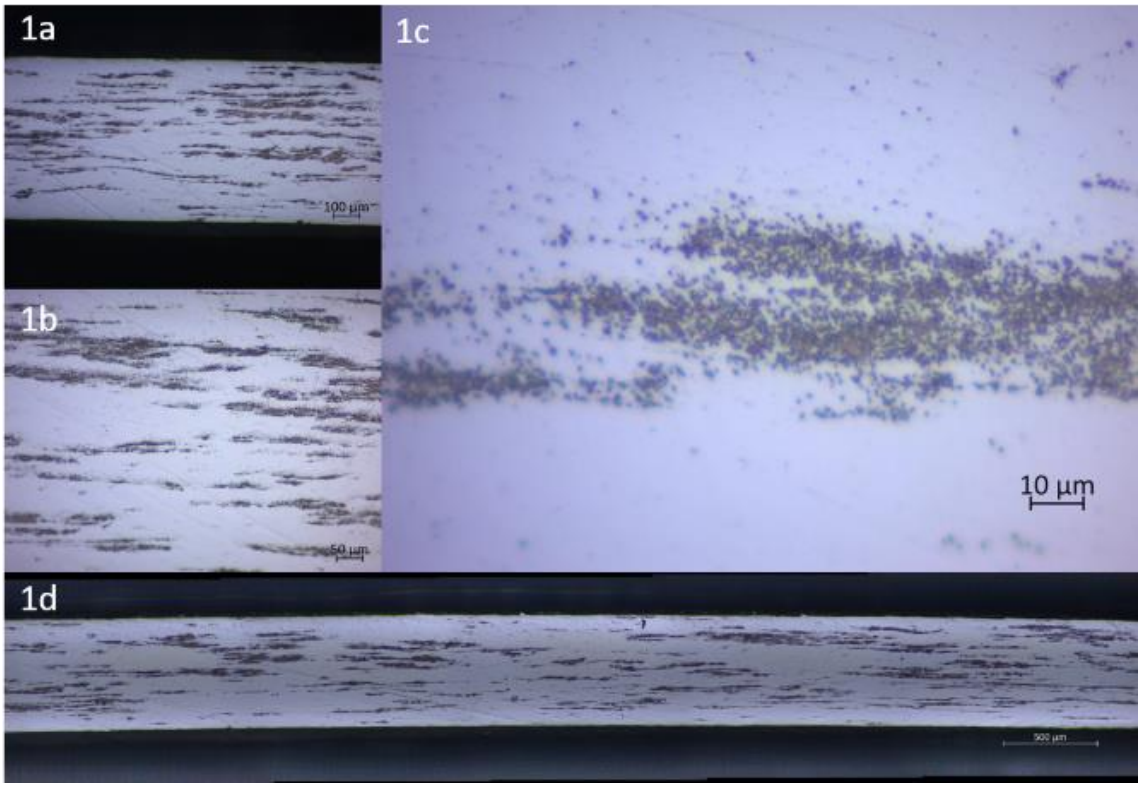

Figure 26 WC nanoparticle dispersion in wires under optical microscope

SEM images further reveal the nature of homogeneous distribution without the sintering of WC nanoparticles in Zn spring wires as shown in figure 2. The brighter particle phases are WC and the darker background is Zn. Figure 2a shows the nanoparticles dispersion in the wire; figure 2b,2c,2d examines if the nanoparticles sinter together.

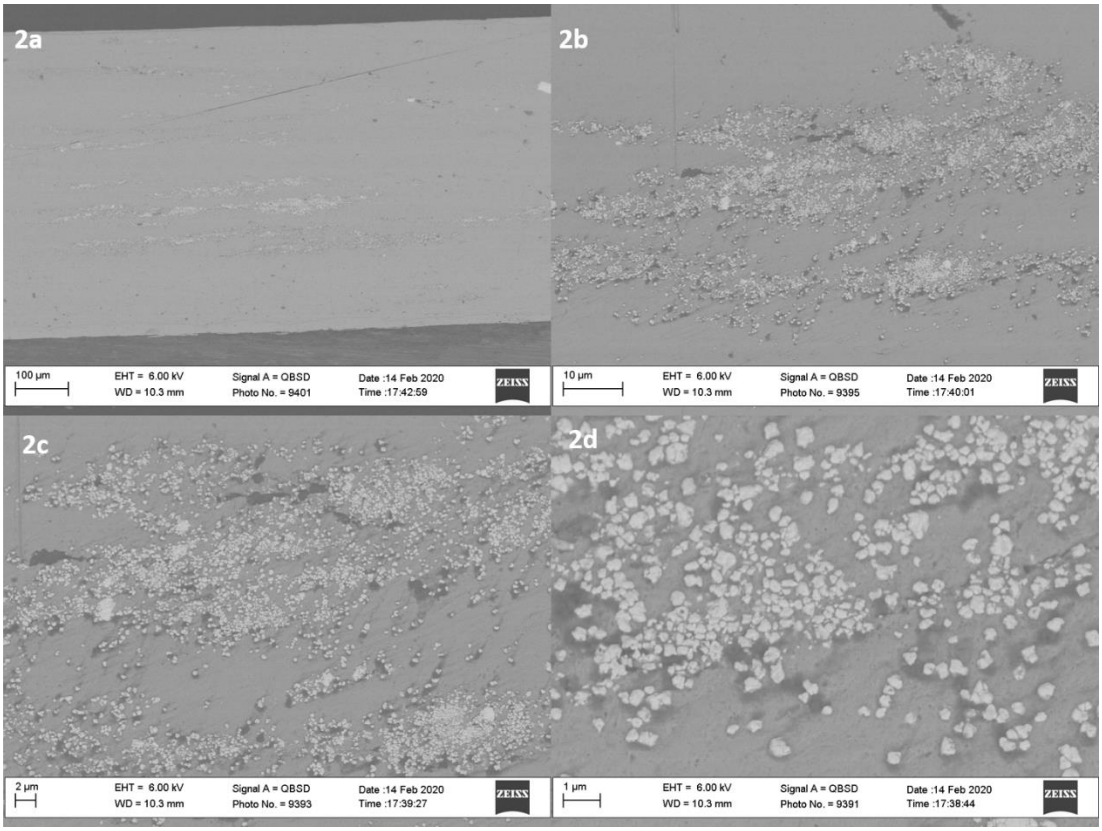

Figure 27 WC nanoparticle dispersion in wires under SEM

For SBS treatment, the requirements for a specific in vivo testing in a porcine subject are that the spring should be able to expand from 2 cm (full compression) to 6 cm (full extension) with an outer diameter of about 14-15mm and a spring constant range between 6N/m and 15N/m. The spring should have such desired geometry as well as adequate extension in order to perform well and achieve jejunal lengthening of porcine subjects in animal testing [93]. In this study, the novel biodegradable Zn-WC springs were designed to fulfill such requirements.

The spring wires used in this study are fabricated through wire-EDM cuttings of the rolled thin Zn-WC plates. Therefore, the cross-section of the spring wire is rectangular, which makes these coiled springs compression die springs. The spring constant *k* of a die spring is dominated by the

geometries of the spring, wire, and the modulus of the wire material, which can be estimated by following equations [97]:

$$k = \frac{Gbt^3}{N_a D^3} K_2 \quad \text{with } \gamma = \frac{E}{2G} - 1 \quad (15)$$

From Equations (15), we can determine:

$$k = \frac{\frac{bt^3 K_2}{2(\gamma+1)}}{N_a D^3} E \quad (16)$$

Where γ is the Poisson's ratio, G is the shear modulus, E is Young's modulus, N_a is the number of active coils, b is the wire cross-section width, t is the wire cross-section length, D is the spring coil mean diameter, and K_2 is the correctional constant for the rectangular cross-section wire. The designed spring constant k for this study following Equation (6) is 6.697N/m with E=73Gpa, γ = 0.256 [98], b=400 µm, t=500 µm, N_a=27-28, D=15mm, and K_2=0.42 [99]. Importantly, Young's Modulus is a critical criterion for biodegradable spring design. By incorporating different volume percentages of WC into the Zn system, the modulus of spring wire material can be manipulated and customized to tune the springs with different spring constants without compromising the geometrical design of the spring, which often is restricted under in-vivo testing and future clinical trials.

Upon coiling up the biodegradable Zn-WC nanocomposite wires into functional springs using a lathe and a mandrel, the spring constants were characterized by compression tests. The compression tests were performed by placing spring vertically in glass tubes and recording the change in spring length as incremental axial loads are directly applied on top of the spring. Each

spring was tested at least 3 times under 4 different axial loads. The calculation of the spring constant k is guided by Hooke's law:

$$F_s = kx \quad (17)$$

Where F_s is the load force compressing the spring while x is the spring compression displacement.

shows the coiling of wires into spring mounted on a mandrel on a lathe; figure 5a shows the spring samples made; figure 5c demonstrate the spring constant k measurement setup

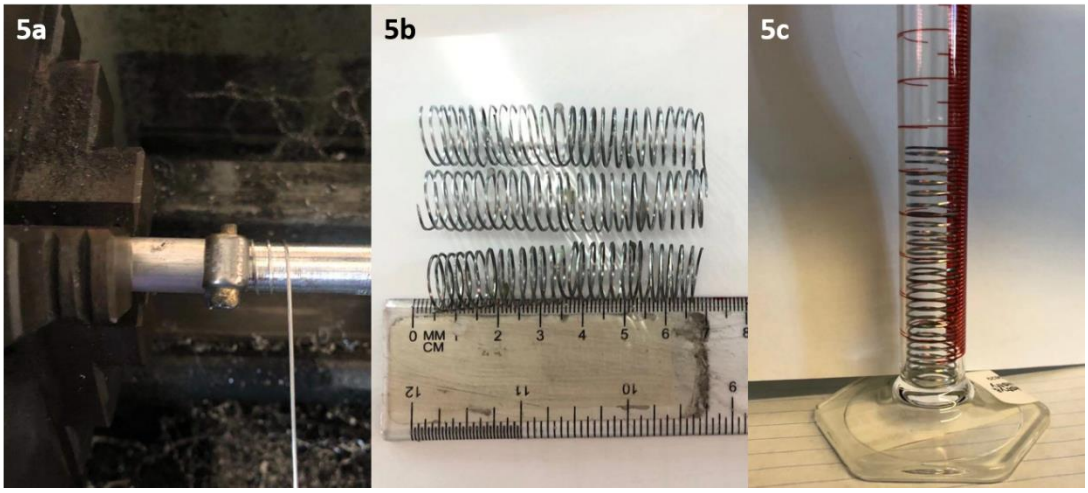

Figure 28 Fabrication and testing of Zn-WC springs

The spring constants determined by the compression tests for three springs are 6.17N/m, c 6.255 N/m, and 6.52 N/m, which match the prediction of the design values well and are satisfactory for the future porcine in vivo degradation test.

Therefore, novel biodegradable Zn-WC springs for the treatment of SBS have been successfully fabricated with enhanced mechanical properties and suitable spring parameters for future animal testing. With its tunable mechanical properties, such as microhardness and Young's

modulus, Zn-WC nanocomposite shows exciting potential to meet future SBS-treating biodegradable spring requirements and challenges without compromising spring geometry design, which is crucial for the implant performances.

Thus, This work presents a successful design and fabrication process of a novel biodegradable spring implant using Zn-WC nanocomposite wires for the potential treatment of SBS. Through characterizations of spring wire material, it is shown that homogeneous nanoparticle distribution is achieved and the mechanical properties are enhanced. Testing of the novel springs demonstrates the feasibility of using biodegradable Zn-WC nanocomposite spring as a new option for SBS-treating. Moreover, it also suggests a promising potential of the Zn-WC nanocomposite as a novel biomaterial. This work also discussed how the tunability of Young's modulus in the Zn-WC nanocomposites can be beneficial for implant spring design.

7.Conclusion and Future work

This study successfully fabricated Zn-based nanocomposite with homogeneous WC nanoparticles dispersion, as well as uniformly incorporated WC nanoparticles into Zn-Fe alloy for the first time. This work has proven that by incorporating WC nanoparticles homogeneously into the Zn and Zn-Fe alloy systems, we can enhance and tune the mechanical properties, such as microhardness and Young's modulus of traditionally weak Zn. The mechanical reinforcement of Zn is significant because Zn, although considered to be the most promising biodegradable material of the decades to come, is inherently lacking mechanical strengths for most of the implant applications. Furthermore, Zn-WC and Zn-Fe-WC nanocomposite present the feasibility to be tuned in mechanical performances to meet various demands from different biomedical applications. By incorporating different volume content of WC nanoparticles into the Zn and Zn-Fe alloy, we could control the degree of enhancement in the mechanical properties of Zn and Zn-Fe alloy. In addition, this work also successfully designed and fabricated a novel biodegradable Zn-WC implant expanding spring for the treatment of short bowel syndrome, a genetic disease that threatens the lives of thousands of newborns every year.

However, Zn matrix nanocomposite, although proven to have superior mechanical strengths, still needs more comprehensive studies. Ceramics nanoparticles such as WC nanoparticles, although inherently benign and inert, have not been studied thoroughly for its impact, if any, on the human health system. Both in vitro and in vivo tests should be conducted on Zn-WC and Zn-Fe-WC system to determine the actual influence of nanocomposite on corrosion behavior, toxicity, and biocompatibility of Zn as a biodegradable material. Future work should also focus on how

nanoparticles affect the natural aging issue of Zn. Zn and its alloy have the tendency to naturally age at room temperature due to its low melting point, which results in loss of ductility during storage. Therefore, a long term study of mechanical ductility of Zn matrix nanocomposite should be conducted to avoid unwanted malfunctions of biodegradable implants.

In addition, more alloy systems, such as Zn-Mg or Zn-Li should be considered for future base materials for Zn matrix nanocomposites, and more possible choices of nanoparticles should be explored to expand the horizon of Zn matrix nanocomposite as biodegradable material.

8.References

[1] E. Mostaed, M. Sikora-Jasinska, J. W. Drelich, and M. Vedani, "Zinc-based alloys for degradable vascular stent applications," *Acta Biomaterialia*, vol. 71, pp. 1–23, Apr. 2018, doi: 10.1016/j.actbio.2018.03.005.

[2] P. K. Bowen, J. Drelich, and J. Goldman, "Zinc Exhibits Ideal Physiological Corrosion Behavior for Bioabsorbable Stents," *Adv. Mater.*, vol. 25, no. 18, pp. 2577–2582, May 2013, doi: 10.1002/adma.201300226.

[3] H. Tapiero and K. D. Tew, "Trace elements in human physiology and pathology: zinc and metallothioneins," *Biomedicine & Pharmacotherapy*, vol. 57, no. 9, pp. 399–411, Nov. 2003, doi: 10.1016/S0753-3322(03)00081-7.

[4] M. Hambidge, "Human Zinc Deficiency," *J Nutr*, vol. 130, no. 5, pp. 1344S-1349S, May 2000, doi: 10.1093/jn/130.5.1344S.

[5] G. Katarivas Levy, J. Goldman, and E. Aghion, "The Prospects of Zinc as a Structural Material for Biodegradable Implants—A Review Paper," *Metals*, vol. 7, no. 10, p. 402, Oct. 2017, doi: 10.3390/met7100402.

[6] J. Niu *et al.*, "Research on a Zn-Cu alloy as a biodegradable material for potential vascular stents application," *Mater Sci Eng C Mater Biol Appl*, vol. 69, pp. 407–413, Dec. 2016, doi: 10.1016/j.msec.2016.06.082.

[7] D. Vojtěch, J. Kubásek, J. Šerák, and P. Novák, "Mechanical and corrosion properties of newly developed biodegradable Zn-based alloys for bone fixation," *Acta Biomaterialia*, vol. 7, no. 9, pp. 3515–3522, Sep. 2011, doi: 10.1016/j.actbio.2011.05.008.

[8] H. Li, H. Yang, Y. Zheng, F. Zhou, K. Qiu, and X. Wang, "Design and characterizations of novel biodegradable ternary Zn-based alloys with IIA nutrient alloying elements Mg, Ca and Sr," *Materials & Design*, vol. 83, pp. 95–102, Oct. 2015, doi: 10.1016/j.matdes.2015.05.089.

[9] M. Sikora-Jasinska, E. Mostaed, A. Mostaed, R. Beanland, D. Mantovani, and M. Vedani, "Fabrication, mechanical properties and in vitro degradation behavior of newly developed ZnAg alloys for degradable implant applications," *Mater Sci Eng C Mater Biol Appl*, vol. 77, pp. 1170–1181, Aug. 2017, doi: 10.1016/j.msec.2017.04.023.

[10] G. Li *et al.*, "Challenges in the use of zinc and its alloys as biodegradable metals: Perspective from biomechanical compatibility," *Acta Biomaterialia*, vol. 97, pp. 23–45, Oct. 2019, doi: 10.1016/j.actbio.2019.07.038.

[11] Z. Guan, S. Pan, C. Linsley, and X. Li, "Manufacturing and Characterization of Zn-WC as Potential Biodegradable Material," *Procedia Manufacturing*, vol. 34, pp. 247–251, 2019, doi: 10.1016/j.promfg.2019.06.146.

[12] L.-Y. Chen *et al.*, "Processing and properties of magnesium containing a dense uniform dispersion of nanoparticles," *Nature*, vol. 528, no. 7583, pp. 539–543, Dec. 2015, doi: 10.1038/nature16445.

[13] N. S. Murni, M. S. Dambatta, S. K. Yeap, G. R. A. Froemming, and H. Hermawan, "Cytotoxicity evaluation of biodegradable Zn-3Mg alloy toward normal human osteoblast cells," *Mater Sci Eng C Mater Biol Appl*, vol. 49, pp. 560–566, Apr. 2015, doi: 10.1016/j.msec.2015.01.056.

[14] J. Kubásek, D. Vojtěch, I. Pospíšilová, A. Michalcova, and J. Maixner, "Microstructure and mechanical properties of the micrograined hypoeutectic Zn–Mg alloy," *International Journal of Minerals, Metallurgy, and Materials*, vol. 23, pp. 1167–1176, Oct. 2016, doi: 10.1007/s12613-016-1336-7.

[15] L. Zhao *et al.*, “Mechanical properties and in vitro biodegradation of newly developed porous Zn scaffolds for biomedical applications,” *Materials & Design*, vol. 108, pp. 136–144, Oct. 2016, doi: 10.1016/j.matdes.2016.06.080.
[16] J. Venezuela and M. S. Dargusch, “The influence of alloying and fabrication techniques on the mechanical properties, biodegradability and biocompatibility of zinc: A comprehensive review,” *Acta Biomaterialia*, vol. 87, pp. 1–40, Mar. 2019, doi: 10.1016/j.actbio.2019.01.035.
[17] P. K. Bowen *et al.*, “Biodegradable Metals for Cardiovascular Stents: from Clinical Concerns to Recent Zn-Alloys,” *Adv. Healthcare Mater.*, vol. 5, no. 10, pp. 1121–1140, May 2016, doi: 10.1002/adhm.201501019.
[18] S. Shadanbaz, J. Walker, T. Woodfield, M. Staiger, and G. Dias, “Monetite and brushite coated magnesium: In vivo and in vitro models for degradation analysis,” *Journal of materials science. Materials in medicine*, vol. 25, Oct. 2013, doi: 10.1007/s10856-013-5059-2.
[19] F. Witte *et al.*, “In vitro and in vivo corrosion measurements of magnesium alloys,” *Biomaterials*, vol. 27, no. 7, pp. 1013–1018, Mar. 2006, doi: 10.1016/j.biomaterials.2005.07.037.
[20] Y.-K. Kim *et al.*, “Gas formation and biological effects of biodegradable magnesium in a preclinical and clinical observation,” *Sci Technol Adv Mater*, vol. 19, no. 1, pp. 324–335, Apr. 2018, doi: 10.1080/14686996.2018.1451717.
[21] Y. F. Zheng, X. N. Gu, and F. Witte, “Biodegradable metals,” *Materials Science and Engineering: R: Reports*, vol. 77, pp. 1–34, Mar. 2014, doi: 10.1016/j.mser.2014.01.001.
[22] M. Peuster, C. Hesse, T. Schloo, C. Fink, P. Beerbaum, and C. von Schnakenburg, “Long-term biocompatibility of a corrodible peripheral iron stent in the porcine descending aorta,” *Biomaterials*, vol. 27, no. 28, pp. 4955–4962, Oct. 2006, doi: 10.1016/j.biomaterials.2006.05.029.
[23] T. Kraus *et al.*, “Biodegradable Fe-based alloys for use in osteosynthesis: Outcome of an in vivo study after 52weeks,” *Acta Biomaterialia*, vol. 10, no. 7, pp. 3346–3353, Jul. 2014, doi: 10.1016/j.actbio.2014.04.007.
[24] D. Pierson *et al.*, “A simplified in vivo approach for evaluating the bioabsorbable behavior of candidate stent materials,” *Journal of Biomedical Materials Research Part B: Applied Biomaterials*, vol. 100B, no. 1, pp. 58–67, 2012, doi: 10.1002/jbm.b.31922.
[25] L. M. Plum, L. Rink, and H. Haase, “The Essential Toxin: Impact of Zinc on Human Health,” *Int J Environ Res Public Health*, vol. 7, no. 4, pp. 1342–1365, Apr. 2010, doi: 10.3390/ijerph7041342.
[26] M. J. Jackson, “Physiology of Zinc: General Aspects,” in *Zinc in Human Biology*, C. F. Mills, Ed. London: Springer, 1989, pp. 1–14.
[27] J.-M. Seitz, M. Durisin, J. Goldman, and J. W. Drelich, “Recent Advances in Biodegradable Metals for Medical Sutures: A Critical Review,” *Advanced Healthcare Materials*, vol. 4, no. 13, pp. 1915–1936, 2015, doi: 10.1002/adhm.201500189.
[28] D. Zhu, Y. Su, M. L. Young, J. Ma, Y. Zheng, and L. Tang, “Biological Responses and Mechanisms of Human Bone Marrow Mesenchymal Stem Cells to Zn and Mg Biomaterials,” *ACS Appl. Mater. Interfaces*, vol. 9, no. 33, pp. 27453–27461, Aug. 2017, doi: 10.1021/acsami.7b06654.
[29] Y. Qiao *et al.*, “Stimulation of bone growth following zinc incorporation into biomaterials,” *Biomaterials*, vol. 35, no. 25, pp. 6882–6897, Aug. 2014, doi: 10.1016/j.biomaterials.2014.04.101.
[30] J. Ma, N. Zhao, and D. Zhu, “Bioabsorbable zinc ion induced biphasic cellular responses in vascular smooth muscle cells,” *Scientific Reports*, vol. 6, no. 1, pp. 1–10, Jun. 2016, doi:

10.1038/srep26661.
[31] P. K. Bowen *et al.*, “Metallic zinc exhibits optimal biocompatibility for bioabsorbable endovascular stents,” *Materials Science and Engineering: C*, vol. 56, pp. 467–472, Nov. 2015, doi: 10.1016/j.msec.2015.07.022.
[32] H. Yang *et al.*, “Evolution of the degradation mechanism of pure zinc stent in the one-year study of rabbit abdominal aorta model,” *Biomaterials*, vol. 145, pp. 92–105, Nov. 2017, doi: 10.1016/j.biomaterials.2017.08.022.
[33] A. Kafri, S. Ovadia, J. Goldman, J. Drelich, and E. Aghion, “The Suitability of Zn–1.3%Fe Alloy as a Biodegradable Implant Material,” *Metals*, vol. 8, no. 3, p. 153, Mar. 2018, doi: 10.3390/met8030153.
[34] I. Hwang, Z. Guan, and X. Li, “Fabrication of Zinc–Tungsten Carbide Nanocomposite Using Cold Compaction Followed by Melting,” *Journal of Manufacturing Science and Engineering*, vol. 140, p. 084503, May 2018, doi: 10.1115/1.4040026.
[35] P. K. Bowen *et al.*, “Evaluation of wrought Zn–Al alloys (1, 3, and 5 wt % Al) through mechanical and in vivo testing for stent applications,” *Journal of Biomedical Materials Research Part B: Applied Biomaterials*, vol. 106, no. 1, pp. 245–258, 2018, doi: 10.1002/jbm.b.33850.
[36] X.-N. Gu and Y.-F. Zheng, “A review on magnesium alloys as biodegradable materials,” *Front. Mater. Sci. China*, vol. 4, no. 2, pp. 111–115, Jun. 2010, doi: 10.1007/s11706-010-0024-1.
[37] E. Mostaed *et al.*, “Novel Zn-based alloys for biodegradable stent applications: Design, development and in vitro degradation,” *Journal of the Mechanical Behavior of Biomedical Materials*, vol. 60, pp. 581–602, Jul. 2016, doi: 10.1016/j.jmbbm.2016.03.018.
[38] C. Rapetto and M. Leoncini, “Magmaris: a new generation metallic sirolimus-eluting fully bioresorbable scaffold: present status and future perspectives,” *Journal of Thoracic Disease*, vol. 9, no. 9, pp. S903-S913–S913, Aug. 2017.
[39] H. Yang *et al.*, “Alloying design of biodegradable zinc as promising bone implants for load-bearing applications,” *Nature Communications*, vol. 11, no. 1, pp. 1–16, Jan. 2020, doi: 10.1038/s41467-019-14153-7.
[40] R. J. Guillory *et al.*, “Corrosion Characteristics Dictate the Long-Term Inflammatory Profile of Degradable Zinc Arterial Implants,” *ACS Biomater. Sci. Eng.*, vol. 2, no. 12, pp. 2355–2364, Dec. 2016, doi: 10.1021/acsbiomaterials.6b00591.
[41] P. Li *et al.*, “Mechanical Characteristics, In Vitro Degradation, Cytotoxicity, and Antibacterial Evaluation of Zn-4.0Ag Alloy as a Biodegradable Material,” *International Journal of Molecular Sciences*, vol. 19, no. 3, p. 755, Mar. 2018, doi: 10.3390/ijms19030755.
[42] H. Gong, K. Wang, R. Strich, and J. G. Zhou, “In vitro biodegradation behavior, mechanical properties, and cytotoxicity of biodegradable Zn–Mg alloy,” *Journal of Biomedical Materials Research Part B: Applied Biomaterials*, vol. 103, no. 8, pp. 1632–1640, 2015, doi: 10.1002/jbm.b.33341.
[43] H. F. Li *et al.*, “Development of biodegradable Zn-1X binary alloys with nutrient alloying elements Mg, Ca and Sr,” *Scientific Reports*, vol. 5, no. 1, pp. 1–14, May 2015, doi: 10.1038/srep10719.
[44] X. Liu *et al.*, “Effects of alloying elements (Ca and Sr) on microstructure, mechanical property and in vitro corrosion behavior of biodegradable Zn–1.5Mg alloy,” *Journal of Alloys and Compounds*, vol. 664, pp. 444–452, Apr. 2016, doi: 10.1016/j.jallcom.2015.10.116.
[45] M. S. Dambatta, S. Izman, D. Kurniawan, and H. Hermawan, “Processing of Zn-3Mg alloy by equal channel angular pressing for biodegradable metal implants,” *Journal of King Saud*

University - Science, vol. 29, no. 4, pp. 455–461, Oct. 2017, doi: 10.1016/j.jksus.2017.07.008.
[46] Z. Tang *et al.*, "Potential biodegradable Zn-Cu binary alloys developed for cardiovascular implant applications," *Journal of the Mechanical Behavior of Biomedical Materials*, vol. 72, pp. 182–191, Aug. 2017, doi: 10.1016/j.jmbbm.2017.05.013.
[47] S. Zhao *et al.*, "Zn-Li alloy after extrusion and drawing: Structural, mechanical characterization, and biodegradation in abdominal aorta of rat," *Materials Science and Engineering: C*, vol. 76, pp. 301–312, Jul. 2017, doi: 10.1016/j.msec.2017.02.167.
[48] S. Sun, Y. Ren, L. Wang, B. Yang, H. Li, and G. Qin, "Abnormal effect of Mn addition on the mechanical properties of as-extruded Zn alloys," *Materials Science and Engineering: A*, vol. 701, pp. 129–133, Jul. 2017, doi: 10.1016/j.msea.2017.06.037.
[49] H. Jin *et al.*, "Novel high-strength, low-alloys Zn-Mg (<0.1wt% Mg) and their arterial biodegradation," *Materials Science and Engineering: C*, vol. 84, pp. 67–79, Mar. 2018, doi: 10.1016/j.msec.2017.11.021.
[50] S. Pan, M. Sokoluk, C. Cao, Z. Guan, and X. Li, "Facile fabrication and enhanced properties of Cu-40 wt% Zn/WC nanocomposite," *Journal of Alloys and Compounds*, vol. 784, pp. 237–243, May 2019, doi: 10.1016/j.jallcom.2019.01.022.
[51] S. Pan, J. Yuan, P. Zhang, M. Sokoluk, G. Yao, and X. Li, "Effect of electron concentration on electrical conductivity in in situ Al-TiB 2 nanocomposites," *Applied Physics Letters*, vol. 116, p. 014102, Jan. 2020, doi: 10.1063/1.5129817.
[52] X. Li, Y. Yang, and X. Cheng, "Ultrasonic-assisted fabrication of metal matrix nanocomposites," *Journal of Materials Science; New York*, vol. 39, no. 9, pp. 3211–3212, May 2004, doi: http://dx.doi.org/10.1023/B:JMSC.0000025862.23609.6f.
[53] M. Malaki *et al.*, "Advanced Metal Matrix Nanocomposites," *Metals*, vol. 9, no. 3, p. 330, Mar. 2019, doi: 10.3390/met9030330.
[54] S. I. Cha, K. T. Kim, S. N. Arshad, C. B. Mo, and S. H. Hong, "Extraordinary Strengthening Effect of Carbon Nanotubes in Metal-Matrix Nanocomposites Processed by Molecular-Level Mixing," *Advanced Materials*, vol. 17, no. 11, pp. 1377–1381, 2005, doi: 10.1002/adma.200401933.
[55] R. Riedel, "Nanoscaled inorganic materials by molecular design," *Chem. Soc. Rev.*, vol. 41, no. 15, pp. 5029–5031, Jul. 2012, doi: 10.1039/C2CS90050E.
[56] R. Casati and M. Vedani, "Metal Matrix Composites Reinforced by Nano-Particles—A Review," *Metals*, vol. 4, no. 1, pp. 65–83, Mar. 2014, doi: 10.3390/met4010065.
[57] P. Calvert, "A recipe for strength," *Nature*, vol. 399, no. 6733, pp. 210–211, May 1999, doi: 10.1038/20326.
[58] T. H. Zhou, W. H. Ruan, J. L. Yang, M. Z. Rong, M. Q. Zhang, and Z. Zhang, "A novel route for improving creep resistance of polymers using nanoparticles," *Composites Science and Technology*, vol. 67, no. 11–12, pp. 2297–2302, Sep. 2007, doi: 10.1016/j.compscitech.2007.01.015.
[59] A. Lekatou *et al.*, "Aluminium reinforced by WC and TiC nanoparticles (ex-situ) and aluminide particles (in-situ): Microstructure, wear and corrosion behaviour," *Materials & Design (1980-2015)*, vol. 65, pp. 1121–1135, Jan. 2015, doi: 10.1016/j.matdes.2014.08.040.
[60] J. Ma, M.-S. Mo, X.-S. Du, P. Rosso, K. Friedrich, and H.-C. Kuan, "Effect of inorganic nanoparticles on mechanical property, fracture toughness and toughening mechanism of two epoxy systems," *Polymer*, vol. 49, no. 16, pp. 3510–3523, Jul. 2008, doi: 10.1016/j.polymer.2008.05.043.
[61] X. Wang, G. Qiao, and Z. Jin, "Fabrication of Machinable Silicon Carbide-Boron Nitride

Ceramic Nanocomposites," *Journal of the American Ceramic Society*, vol. 87, no. 4, pp. 565–570, 2004, doi: 10.1111/j.1551-2916.2004.00565.x.
[62] M. Sokoluk, C. Cao, S. Pan, and X. Li, "Nanoparticle-enabled phase control for arc welding of unweldable aluminum alloy 7075," *Nature Communications*, vol. 10, no. 1, pp. 1–8, Jan. 2019, doi: 10.1038/s41467-018-07989-y.
[63] M. Kireitseu, D. Hui, and G. Tomlinson, "Advanced shock-resistant and vibration damping of nanoparticle-reinforced composite material," *Composites Part B: Engineering*, vol. 39, no. 1, pp. 128–138, Jan. 2008, doi: 10.1016/j.compositesb.2007.03.004.
[64] D. L. Burris and W. G. Sawyer, "Improved wear resistance in alumina-PTFE nanocomposites with irregular shaped nanoparticles," *Wear*, vol. 260, no. 7, pp. 915–918, Apr. 2006, doi: 10.1016/j.wear.2005.06.009.
[65] G. Liu *et al.*, "Nanostructured high-strength molybdenum alloys with unprecedented tensile ductility," *Nature Materials*, vol. 12, no. 4, pp. 344–350, Apr. 2013, doi: 10.1038/nmat3544.
[66] W. S. Miller and F. J. Humphreys, "Strengthening mechanisms in particulate metal matrix composites," *Scripta Metallurgica et Materialia*, vol. 25, no. 1, pp. 33–38, Jan. 1991, doi: 10.1016/0956-716X(91)90349-6.
[67] L. H. Dai, Z. Ling, and Y. L. Bai, "Size-dependent inelastic behavior of particle-reinforced metal–matrix composites," *Composites Science and Technology*, vol. 61, no. 8, pp. 1057–1063, Jun. 2001, doi: 10.1016/S0266-3538(00)00235-9.
[68] D. C. Dunand and A. Mortensen, "On plastic relaxation of thermal stresses in reinforced metals," *Acta Metallurgica et Materialia*, vol. 39, no. 2, pp. 127–139, Feb. 1991, doi: 10.1016/0956-7151(91)90261-X.
[69] H. J. Choi, Y. Kim, J. H. Shin, and D. H. Bae, "Deformation behavior of magnesium in the grain size spectrum from nano- to micrometer," *Materials Science and Engineering: A*, vol. 527, no. 6, pp. 1565–1570, Mar. 2010, doi: 10.1016/j.msea.2009.10.035.
[70] V. C. Nardone and K. M. Prewo, "On the strength of discontinuous silicon carbide reinforced aluminum composites," *Scripta Metallurgica*, vol. 20, no. 1, pp. 43–48, Jan. 1986, doi: 10.1016/0036-9748(86)90210-3.
[71] J. Moon, S. Kim, J. Jang, J. Lee, and C. Lee, "Orowan strengthening effect on the nanoindentation hardness of the ferrite matrix in microalloyed steels," *Materials Science and Engineering: A*, vol. 487, no. 1, pp. 552–557, Jul. 2008, doi: 10.1016/j.msea.2007.10.046.
[72] C. H. Cáceres, J. R. Griffiths, A. R. Pakdel, and C. J. Davidson, "Microhardness mapping and the hardness-yield strength relationship in high-pressure diecast magnesium alloy AZ91," *Materials Science and Engineering: A*, vol. 402, no. 1, pp. 258–268, Aug. 2005, doi: 10.1016/j.msea.2005.04.042.
[73] H. Yang, L. Jiang, M. Balog, P. Krizik, and J. M. Schoenung, "Reinforcement Size Dependence of Load Bearing Capacity in Ultrafine-Grained Metal Matrix Composites," *Metall and Mat Trans A*, vol. 48, no. 9, pp. 4385–4392, Sep. 2017, doi: 10.1007/s11661-017-4186-7.
[74] G. C. Eckold, *Design and Manufacture of Composite Structures*. Woodhead Publishing, 1994.
[75] S. C. Tjong, "Novel Nanoparticle-Reinforced Metal Matrix Composites with Enhanced Mechanical Properties," *Advanced Engineering Materials*, vol. 9, no. 8, pp. 639–652, 2007, doi: 10.1002/adem.200700106.
[76] Y. Yang, J. Lan, and X. Li, "Study on bulk aluminum matrix nano-composite fabricated by ultrasonic dispersion of nano-sized SiC particles in molten aluminum alloy," *Materials*

Science and Engineering: A, vol. 380, no. 1, pp. 378–383, Aug. 2004, doi: 10.1016/j.msea.2004.03.073.
[77] J. Lan, Y. Yang, and X. Li, "Microstructure and microhardness of SiC nanoparticles reinforced magnesium composites fabricated by ultrasonic method," *Materials Science and Engineering: A*, vol. 386, no. 1, pp. 284–290, Nov. 2004, doi: 10.1016/j.msea.2004.07.024.
[78] J. Hemanth, "Development and property evaluation of aluminum alloy reinforced with nano-ZrO2 metal matrix composites (NMMCs)," *Materials Science and Engineering: A*, vol. 507, no. 1, pp. 110–113, May 2009, doi: 10.1016/j.msea.2008.11.039.
[79] A. Dehghan Hamedan and M. Shahmiri, "Production of A356–1wt% SiC nanocomposite by the modified stir casting method," *Materials Science and Engineering: A*, vol. 556, pp. 921–926, Oct. 2012, doi: 10.1016/j.msea.2012.07.093.
[80] M. Gupta and S. N. M. Ling, *Magnesium, Magnesium Alloys, and Magnesium Composites*. John Wiley & Sons, 2011.
[81] K. M. Mussert, W. P. Vellinga, A. Bakker, and S. Van Der Zwaag, "A nano-indentation study on the mechanical behaviour of the matrix material in an AA6061 - Al2O3 MMC," *Journal of Materials Science*, vol. 37, no. 4, pp. 789–794, Feb. 2002, doi: 10.1023/A:1013896032331.
[82] J. N. Israelachvili, "Intermolecular and Surface Forces," p. 706.
[83] A. Contreras, C. A. León, R. A. L. Drew, and E. Bedolla, "Wettability and spreading kinetics of Al and Mg on TiC," *Scripta Materialia*, vol. 48, no. 12, pp. 1625–1630, Jun. 2003, doi: 10.1016/S1359-6462(03)00137-4.
[84] I. Egry, E. Ricci, R. Novakovic, and S. Ozawa, "Surface tension of liquid metals and alloys — Recent developments," *Advances in Colloid and Interface Science*, vol. 159, no. 2, pp. 198–212, Sep. 2010, doi: 10.1016/j.cis.2010.06.009.
[85] I. Hwang, Z. Guan, and X. Li, "Scalable Manufacturing of Zinc-Tungsten Carbide Nanocomposites," *Procedia Manufacturing*, vol. 26, pp. 140–145, Jan. 2018, doi: 10.1016/j.promfg.2018.07.017.
[86] P. Blau, *Wear of Materials*. Elsevier, 2003.
[87] R. Waksman, R. Pakala, R. Baffour, R. Seabron, D. Hellinga, and F. O. Tio, "Short-term effects of biocorrodible iron stents in porcine coronary arteries," *J Interv Cardiol*, vol. 21, no. 1, pp. 15–20, Feb. 2008, doi: 10.1111/j.1540-8183.2007.00319.x.
[88] A. Kafri, S. Ovadia, G. Yosafovich-Doitch, and E. Aghion, "In vivo performances of pure Zn and Zn–Fe alloy as biodegradable implants," *J Mater Sci: Mater Med*, vol. 29, no. 7, p. 94, Jul. 2018, doi: 10.1007/s10856-018-6096-7.
[89] K. Han, I. Ohnuma, K. Okuda, and R. Kainuma, "Experimental determination of phase diagram in the Zn-Fe binary system," *Journal of Alloys and Compounds*, vol. 737, pp. 490–504, Mar. 2018, doi: 10.1016/j.jallcom.2017.11.320.
[90] J. G. Miranda-Hernández, H. Herrera-Hernández, C. O. González-Morán, J. N. Rivera Olvera, I. Estrada-Guel, and F. Botello Villa, "Synthesis and Characterization of Zn-Nix Advanced Alloys Prepared by Mechanical Milling and Sintering at Solid-State Process," *Advances in Materials Science and Engineering*, 2017. [Online]. Available: https://www.hindawi.com/journals/amse/2017/7967848/. [Accessed: 27-Feb-2020].
[91] J. A. Vanderhoof and A. N. Langnas, "Short-bowel syndrome in children and adults," *Gastroenterology*, vol. 113, no. 5, pp. 1767–1778, Nov. 1997, doi: 10.1053/gast.1997.v113.pm9352883.
[92] S. J. D. O'Keefe, A. L. Buchman, T. M. Fishbein, K. N. Jeejeebhoy, P. B. Jeppesen, and

J. Shaffer, “Short bowel syndrome and intestinal failure: consensus definitions and overview,” *Clin. Gastroenterol. Hepatol.*, vol. 4, no. 1, pp. 6–10, Jan. 2006, doi: 10.1016/j.cgh.2005.10.002.
[93] N. Huynh *et al.*, “Spring-mediated distraction enterogenesis in-continuity,” *Journal of Pediatric Surgery*, vol. 51, no. 12, pp. 1983–1987, Dec. 2016, doi: 10.1016/j.jpedsurg.2016.09.024.
[94] A. Scott *et al.*, “Mechanical lengthening in multiple intestinal segments in-series,” *Journal of Pediatric Surgery*, vol. 51, no. 6, pp. 957–959, Jun. 2016, doi: 10.1016/j.jpedsurg.2016.02.058.
[95] N. Huynh *et al.*, “Three-dimensionally printed surface features to anchor endoluminal spring for distraction enterogenesis,” *PLOS ONE*, vol. 13, no. 7, p. e0200529, Jul. 2018, doi: 10.1371/journal.pone.0200529.
[96] L.-Y. Chen, J.-Y. Peng, J.-Q. Xu, H. Choi, and X.-C. Li, “Achieving uniform distribution and dispersion of a high percentage of nanoparticles in metal matrix nanocomposites by solidification processing,” *Scripta Materialia*, vol. 69, no. 8, pp. 634–637, Oct. 2013, doi: 10.1016/j.scriptamat.2013.07.016.
[97] A. M. Wahl, *Mechanical springs.* New York: McGraw-Hill, 1963.
[98] H. M. Ledbetter, “Elastic properties of zinc: A compilation and a review,” *Journal of Physical and Chemical Reference Data*, vol. 6, no. 4, pp. 1181–1203, Oct. 1977, doi: 10.1063/1.555564.
[99] W. R. Berry, *Spring Design: A Practical Treatment*. Emmott, 1961.